Proceedings of the Estonian Academy of Sciences,
2024, **73**, 3, 279–316
https://doi.org/10.3176/proc.2024.3.11
Available online at www.eap.ee/proceedings

NUMERICAL
SIMULATION IN
MECHANICS

A review of temporal and spatial dispersions of linear and quadratic finite elements in linear elastic wave propagation problems

Radek Kolman[a,b], Miloslav Okrouhlík[a,b] and Alena Kruisová[a*]

[a] Institute of Thermomechanics, Czech Academy of Sciences, Dolejškova 1402/5, 182 00 Prague 8, Czech Republic
[b] College of Polytechnics Jihlava, Tolstého 16, 586 01 Jihlava, Czech Republic

Received 24 February 2024, accepted 27 March 2024, available online 19 August 2024

Abstract. The dispersion behaviour of the finite element method, applied to the treatment of stress wave propagation tasks in an elastic solid continuum, is reviewed and complemented with the authors' contributions in the field, along with substantial details of finite element technology. It is shown how finite element dispersion disqualifies to a certain extent the stress wave propagation modelling and, as such, cannot be completely eradicated. The paper, however, reveals the ways how the dispersion effect (actually, modelling errors) could be minimized. The effects of spatial and temporal dispersions of the finite element method are treated. 1D and 2D linear and quadratic finite elements and their suitability are analysed for use with implicit and explicit integration methods. Historical as well as new, up-to-date approaches are also reviewed. The paper closes with recommendations for values of mesh size and timestep size, mass matrices and direct time integrations with respect to dispersion errors in finite element modelling of elastic wave propagation problems in solids.

Keywords: dispersion, elastic wave propagation, finite element method, direct time integration, spurious oscillations.

1. INTRODUCTION

In general, dispersion is a phenomenon characterized by the fact that the velocity of a propagating wave depends on its frequency. Dispersion behaviour is observed not only in several materials with microstructures, metamaterials, porous materials, thin-walled structures and dispersive fluids but also as the numerical phenomenon of numerical methods in continuum mechanics.

In this paper, attention is given to the theory underpinning dispersion phenomena in computational solid mechanics. We intend to describe dispersion effects when using the finite element method (FEM) to model wave propagation tasks. A study of this subject allows us to understand and thereby minimize the computational complications encountered when applying FEM to non-stationary dynamics tasks for solid computational mechanics. Our approach to dispersion analysis also facilitates safe estimation of the 'correct' mesh size and timestep size. We provide safe choices for the model's numerical parameters.

The standard computational approaches currently used in continuum mechanics are based on discretization in space and time. In continuum mechanics, the finite element, finite volume, boundary element and

* Corresponding author, alena@it.cas.cz

other methods that involve explicit and implicit time stepping are typical examples of actual numerical approaches. In this paper, we will show that FEM is discrete in nature and that the results of wave propagation tasks are substantially influenced by dispersion side effects.

FEM dispersion behaviour encompasses change of direction and wave speeds. It affects, in general, the way in which waves propagate. Furthermore, the FEM mesh behaves as a frequency filter, meaning that not all the frequencies can be transmitted. Wave propagation in lattice structures, mass-spring systems and finite element (FE) discretized systems can be observed to be strongly analogous.

Even if embedded flaws cannot be fully eliminated, we will show how they can at least be minimized. Though the subject of spatial and temporal dispersion in discretized solid continuum mechanics might seem academic and theoretical, it nevertheless has practical ramifications for current users of commercial FE packages. Knowledgeable users should be able to minimize dispersion side effects by skillfully choosing appropriate element and mass matrix types, mesh densities and time integration methods with the correct timestep size, etc. For that reason, the dispersive behaviour of the numerical model should be analysed and the basic numerical parameters suggested so that numerical modelling using FEM can be sufficiently accurate. From the beginning of its history, with Alexander Hrennikoff (1941) and Richard Courant (1943), many authors have studied the finite element method and published their results as they relate to the many effects and variants of FEM and their relation to dispersive properties. In the following text, we mention several works related to this subject. The results we present on the dispersive properties of FEM are based on systematic works of the numerical group from the Institute of Thermomechanics, Czech Academy of Sciences.

Chin (1975) formerly presented a mathematical framework for dispersion analysis of FEM, based on solving hyperbolic partial differential equations (PDEs). He observed the Gibb's phenomenon in the FEM solution. Subsequently, others used the Fourier method (sometimes called the Von Neumann method) as the dispersion analysis tool. An efficient approach to the complex wave numbers Fourier analysis of FEM was later introduced by Thompson and Pinsky (1995).

Krieg and Key (1973) studied the one-dimensional constant strain elements employed in the numerical elucidation of the one-dimensional Helmholtz equation. They discovered a relationship between mass matrix type and temporal discretization. Belytschko and Mullen (1978) extended this dispersion analysis to higher-order (quadratic) one-dimensional elements. It was shown that a so-called optical branch existed in the spectrum. This notion referred to the original text of Brillouin (1953), in which the lowest characteristics were called the *acoustic* branches and the higher ones, the *optical* branches. In that well-known study, the dispersion analysis revealed the 'stopping' bands in the frequency spectrum of biquadratic elements whose corresponding solutions in the frequency range decayed exponentially due to the attenuation effect of *band-gap structures*. Along the sidelines, one-dimensional higher-order Langrangian and Hermitian elements were studied by Okrouhlík and Höschl (1993). The following types of shape functions were considered: Legendre polynomials (hp-version of FEM) and hierarchic Fourier functions (Thompson and Pinsky 1995), Chebyshev polynomials (Dauksher and Emery 1997, 2000; Seriani 2004; Seriani and Oliveira 2008), B-splines (Vichnevetsky and Bowles 1982; Kwok et al. 2001) or NURBS (non-uniform rational B-splines) (Cottrell et al. 2006; Hughes et al. 2008). The effects of non-homogeneities and parametrization of B-spline shape functions on dispersion and attenuation behaviour were studied by Kolman et al. (2014) and are presented here.

Holmes and Belytschko (1976) showed numerically that an abrupt change of mesh size produced interior reflections, contributing to the propagation of spurious waves. Their magnitude was analytically studied by Bažant and Celep (1982). The same authors subsequently proved in the work led by Celep and Bažant (1982) that mesh grading (i.e. the insertion of a transition domain) did not provide much assistance as it could not absorb the spurious modes. Mullen and Belytschko (1982) extended the dispersion analysis to two-dimensional wave equations using bilinear elements, where the effects of mesh layout, mass approximation and under-integration were examined. The dispersion properties of triangular, rectangular and square finite elements for two-dimensional domains have been determined and analysed by Brepta and Okrouhlík (1984, 1986). Abboud and Pinsky (1992) carried out dispersion analysis of the three-dimensional second-order

scalar wave equation (the three-dimensional Helmholtz equation). The analysis was performed for trilinear rectangular 8-node elements, for triquadratic rectangular 27-node elements and for serendipity rectangular 20-node elements with the additional investigation of mass approximation. Liu et al. (1994) studied the effect of distortion of linear elements. In Christon (1999), the influence of the mass matrix approximation on dispersion was outlined. Brepta et al. (1996) and Červ et al. (1996) used FEM to investigate the dispersion of harmonic Raleigh waves propagating along a straight boundary formed by a thin, elastic solid.

Other discoveries in this field included the Newmark and central difference methods, the former enabling a full (combined temporal and spatial) dispersion analysis and the latter considering both consistent and lumped mass matrices. It was additionally shown that the dispersion relations for time integration numerical schemes were influenced by the magnitude of the timestep. Based on this analysis, the Newmark method was recognised as the best match for a consistent mass matrix, while the central difference method was a suitable counterpart for mass lumping procedures. For different time schemes, Marfurt (1984) examined the accuracy of the finite difference method (FDM) and FEM when applied to scalar and elastic wave equations. Schreyer (1983) contributed to the application of dispersion analysis to fully discretized systems.

The wave component-decomposition method with pull-back interpolation for the elimination of numerical dispersion has been presented in Cho et al. (2013, 2019). In this method, each type of wave component is integrated with different timestep sizes for longitudinal and shear waves of different wave speeds (see also Kolman et al. 2016a). Here, each type of wave component is integrated with different timestep sizes accounting for the different wave speeds for longitudinal and shear waves.

Our present contribution is to devote our attention to the dispersion behaviour of classical finite elements and the effect of temporal-spatial discretization and mass matrix type. We do this in the format of a review paper.

2. GOVERNING EQUATIONS OF WAVE PROPAGATION IN ELASTIC SOLIDS

The subject of linear elastic wave propagation in solids is based on assumptions of linear continuum mechanics, i.e. engineering stress, small strains and small displacements, linear relation between strains and derivatives of displacements and the linear relation between stresses and strains (see Love 1944; Kolsky 1953; Davies 1956; Brillouin 1953; Zukas 1990). The quantities we are dealing with are the engineering stress and the infinitesimal Cauchy strain (also called the engineering strain).

We assume a body occupying the bounded domain $\Omega \subset \mathbf{R}^3$ with the boundary $\partial\Omega$. The governing equations – the balance of linear momentum at the material particle level – consist of the equations of motion, relating the internal and inertia effects, and neglected volume forces, i.e. yields to

$$\frac{\partial \sigma_{ji}}{\partial x_j} = \rho \frac{\partial^2 u_i}{\partial t^2} \qquad \text{on } \Omega \tag{1}$$

of the Cauchy kinematic equations, describing the relation between the engineering strain and the first derivative of displacements, i.e.

$$\varepsilon_{ij} = \frac{1}{2}\left(\frac{\partial u_i}{\partial x_j} + \frac{\partial u_j}{\partial x_i}\right) \tag{2}$$

and, finally, of the linear relation between the engineering stress and engineering strain, represented by Hooke's law, i.e.

$$\sigma_{ij} = C_{ijkl}\varepsilon_{kl}. \tag{3}$$

In the governing equations, Eqs (1) to (3), the quantity σ_{ij} stands for the engineering stress components, ρ is the density, ε_{ij} stands for the Cauchy strain components, the components u_i represent the displacement vector $\mathbf{u}(\mathbf{x},\mathbf{t})$, the components of the fourth-order tensor of elasticity C_{ijkl} contain the elastic moduli and, finally, x_i and t are the spatial coordinate and time, respectively. Of course, the PDE system should be

supplemented with the Dirichlet and Neumann boundary conditions on the boundary $\partial\Omega$ as well as the initial conditions of the given positions and velocities at the initial time of interest.

In the text of this paper, the attributes 'engineering' and/or 'infinitesimal' will not be emphasized further, as in Achenbach (1973). We also assume an unbounded domain of interest $\Omega = \mathbf{R}^3$ of isotropic and homogeneous media for dispersion analysis of FEM in wave propagation.

2.1. Plane wave propagation and definition of basic quantities in wave propagation

For the dispersion analysis, we assume a special case of motion. One may consider a plane harmonic solution to Eq. (1) for an unbounded domain as in Brillouin (1953) and Achenbach (1973):

$$\mathbf{u}(\mathbf{x},t) = \mathbf{U}\exp[\mathrm{i}\ (\mathbf{k}\mathbf{x} \pm \omega t)], \tag{4}$$

where $\mathbf{U} = (U_x, U_y, U_z)$ is the amplitude vector, $\mathrm{i} = \sqrt{-1}$ is the imaginary unit, $\mathbf{k} = (k_x, k_y, k_z)$ is the wave vector and ω is the angular velocity. The polarization vector $\mathbf{U}$ for the longitudinal wave is satisfying the condition $\mathbf{U} \parallel \mathbf{k}$ and $\mathbf{U} \perp \mathbf{k}$ for the transversal wave. For a given wave length λ, the wave number $k = |\mathbf{k}|$ may be computed from

$$k = \frac{2\pi}{\lambda}. \tag{5}$$

The vector of phase velocity $\mathbf{c}$ is related to angular velocity ω and k by

$$\mathbf{c} = \left(\frac{\omega}{k_x}, \frac{\omega}{k_y}, \frac{\omega}{k_z}\right) \tag{6}$$

with the amplitude $c = |\mathbf{c}|$. The vector of group velocity $\mathbf{c}_g$ is defined by Achenbach (1973) as

$$\mathbf{c}_g = \frac{\mathrm{d}\omega}{\mathrm{d}\mathbf{k}} = \left(\frac{\partial\omega}{\partial k_x}, \frac{\partial\omega}{\partial k_y}, \frac{\partial\omega}{\partial k_z}\right) \tag{7}$$

with the amplitude $c_g = |\mathbf{c}_g|$. The period of harmonic motion at the point is defined as $T = 2\pi/\omega$.

In non-dispersive systems, the dispersion relationship $\omega = f(\mathbf{k})$ is prescribed by the linear function $\omega = c\,k$ and then $c_g = c$. Thus, in the absence of dispersion, the group velocity equals the phase velocity, and c and c_g are constants. This medium is also isotropic – the phase and group velocities are independent of the direction of wave propagation. In a dispersive medium, the dispersion relationship $\omega = f(\mathbf{k})$ is not a linear function, and the group velocity $\mathbf{c}_g$ should be associated with a different direction than the wave vector $\mathbf{k}$.

2.2. Wave speed in 1D

In 1D space, the propagating elastic wave, in terms of displacements, is described by the so-called 1D wave equation in the form

$$\frac{\partial^2 u}{\partial t^2} = c_0^2 \frac{\partial^2 u}{\partial x^2} \qquad \text{on } \mathbf{R}, \tag{8}$$

where u is the longitudinal displacement, $c_0 = \sqrt{E/\rho}$ is the speed of propagation, x and t are the longitudinal displacement and time, respectively. The solution of Eq. (8), the distribution of longitudinal displacements in time and space, could be assumed in the form

$$u(x,t) = f(x \pm c_0 t). \tag{9}$$

The distribution of stress and strain components is subsequently computed using Eqs (2) and (3). It should be emphasized that in the linear theory of elasticity, when we talk about stress waves, the strain and stress waves are linear combinations of the displacement distribution. Furthermore, the histories of velocity and acceleration are evaluated by differentiating the displacement distribution with respect to time.

The term f, appearing in Eq. (9), is an arbitrary function satisfying certain continuity conditions (see Brillouin 1953). The resulting solution is independent of the frequency of the propagating wave. In other words, in a 1D solid continuum, the stress waves of all frequencies propagate with the same speed, i.e. c_0. So, a wave package, generally composed of the whole spectrum of frequencies, propagates in time and space without any distortion. In this respect, the 1D solid continuum is defined as the *dispersionless medium*, meaning that **all the harmonic waves, regardless of their frequencies, propagate with the same speed.** In other words, this model is dispersionless.

In this paper, we focus only on wave propagation in elastic media. In one-dimensional media described by the linear wave equation, the solution does not exhibit dispersion behaviour. However, there are many models and model corrections in 1D wave propagation that can describe the dispersion wave propagation as elastic wave propagation in a long cylinder with radial displacement correction, dispersion waves in nerves or soliton wave propagation. For more details, see the book by Engelbrecht (2015).

2.3. Wave speeds in 2D – plane stress case

When considering the plane state of stress and eliminating the stress variables from Eqs (1) to (3), and using scalar notation with displacements u, v defined in the directions x, y, we get the so-called Lamé's wave equations of motion for the isotropic and homogeneous media (Love 1944). They have the form on $\mathbf{R}^2$:

$$\rho \frac{\partial^2 u}{\partial t^2} = \frac{E}{1-\mu^2}\left[\frac{\partial^2 u}{\partial x^2} + \mu \frac{\partial^2 v}{\partial x \partial y}\right] + G\left[\frac{\partial^2 u}{\partial y^2} + \frac{\partial^2 v}{\partial x \partial y}\right], \tag{10}$$

$$\rho \frac{\partial^2 v}{\partial t^2} = \frac{E}{1-\mu^2}\left[\frac{\partial^2 v}{\partial y^2} + \mu \frac{\partial^2 u}{\partial x \partial y}\right] + G\left[\frac{\partial^2 v}{\partial x^2} + \frac{\partial^2 u}{\partial x \partial y}\right], \tag{11}$$

where μ is the Poisson's ratio and E, G are the Young's and shear moduli, respectively. In this case, there are two types of wave propagation through the unbounded isotropic and homogeneous domain. The wave pattern, in terms of displacement components, i.e. the solution of Eqs (10) and (11), can be described by two arbitrary functions f and h (see Brillouin 1953). Only the argument with the minus sign is considered since the functions with the plus sign argument represent identical waves travelling in opposite directions:

$$u = f(x - c_3 t), \qquad v = h(y - c_3 t). \tag{12}$$

This wave is called *longitudinal* (also P, primary, dilatational, irrotational or extensional) and propagates with the speed

$$c_3 = \sqrt{\frac{E}{\rho(1-\mu^2)}}. \tag{13}$$

The wave pattern, in terms of displacement components, i.e. the solution Eq. (11), can be described by arbitrary functions

$$u = F(y - c_2 t), \qquad v = H(x - c_2 t). \tag{14}$$

This wave is called *transversal* (also S, shear, rotational, equivolumetrical) and propagates with the speed

$$c_2 = \sqrt{\frac{G}{\rho}}. \tag{15}$$

In a 2D continuum, the longitudinal and transversal waves propagate at different speeds. In an unbound domain, the waves are not coupled and are independent of their frequencies. Geometrically, the displacement vector of the longitudinal wave has the direction of the wave propagation direction. The displacement of the shear wave is perpendicular to the direction of wave propagation (see Kolsky 1953).

2.4. Wave speeds in 2D – plane strain case

The equations of motion are the same as before, but under plane strain conditions, **the speed of longitudinal waves is** $c_1 = \sqrt{\frac{E}{\rho}\frac{1-\mu}{(1+\mu)(1-2\mu)}}$, while the **speed of transversal waves** is the same as for the plane state of stress, i.e. $c_2 = \sqrt{\frac{G}{\rho}}$. For more details, see Love (1944). So, **the unbound 2D continuum, regardless of the plane stress or plain strain conditions, is a dispersionless medium.**

2.5. Wave speeds in 3D

For the three-dimensional task of elastodynamics with the isotropic and homogeneous media, the governing equations in the operator notation have the form

$$(\Lambda + G)\,\mathrm{grad}\,\mathrm{div}\,\mathbf{u} + G\triangle\mathbf{u} = \rho\frac{\partial^2\mathbf{u}}{\partial t^2} \qquad \text{on } \mathbf{R}^3, \tag{16}$$

where $\triangle$ marks the Laplace operator and Λ and G are the Lamé's constants. The Lamé's constants Λ, G may be related to the engineering constants E, μ as

$$\Lambda = \frac{\mu E}{(1+\mu)(1-2\mu)}, \qquad G = \frac{E}{2(1+\mu)}. \tag{17}$$

As in the 2D space, in a 3D unbound continuum, the longitudinal and transversal waves are not coupled and propagate at different speeds. The speeds are c_1 and c_2, respectively. In an unbound medium, the waves are independent of their frequency as well. So, the **unbound 3D continuum is also the dispersionless medium** (see Love 1944). The geometry of wave propagation modes is the same as for the 2D problem. However, we have two shear waves that are perpendicular amplitude vectors to each other.

2.6. Examples of values of wave speeds for different spatial statuses

As we said, in a 1D continuum, there is only a single speed of wave propagation, i.e. $c_0 = \sqrt{E/\rho}$. Due to the existence of normal and shear stresses in 2D and 3D continua, there are two kinds of stress waves that could propagate in an unbound medium in a non-dispersive way (see Kolsky 1953). These are *longitudinal* (P, *primary*) and *transversal* (S, *shear*) waves – their speeds are different. The speed formulas and values (in m/s) for a typical steel material with the Young modulus ($E = 2.1 \times 10^{11}$ Pa, density $\rho = 7600\ \mathrm{kg/m^3}$, Poisson's ratio $\mu = 0.3$) are as follows:

$$\begin{aligned}
&\text{1D wave, slender rod:}\\
&c_0 = \sqrt{E/\rho} = 5189\ [\mathrm{m/s}];\\
&\text{P wave for 2D plane strain and for 3D problems:}\\
&c_1 = \sqrt{(2G+\Lambda)/\rho} = 6020\ [\mathrm{m/s}],\\
&\text{where } \Lambda = \tfrac{\mu E}{(1+\mu)(1-2\mu)},\ G = \tfrac{E}{2(1+\mu)};\\
&\text{P wave for 2D plane stress problem:}\\
&c_3 = \sqrt{E/(\rho(1-\mu^2))} = 5439\ [\mathrm{m/s}];\\
&\text{S wave, shear, both for 2D and 3D problems:}\\
&c_2 = \sqrt{G/\rho} = 3218\ [\mathrm{m/s}].
\end{aligned} \tag{18}$$

The following text will be devoted to the numerical modelling of wave propagation for elastic waves and to numerical errors arising from numerical solutions obtained by the finite element method.

3. FINITE ELEMENT METHOD FOR ELASTIC WAVE PROPAGATION

The finite element treatment of transient tasks in elastodynamics is based on equations of motion that have the form of second-order linear ordinary differential equations with constant coefficients. When no damping is considered, the equations of motion of the whole body (structure) – for the displacement-based FE formulation – in the matrix form have the form

$$\mathbf{M}\ddot{\mathbf{q}} + \mathbf{K}\mathbf{q} = \mathbf{F}(t), \tag{19}$$

where $\mathbf{M}$ is the global mass matrix, $\mathbf{K}$ denotes the global stiffness matrix, column arrays $\mathbf{q}$ and $\ddot{\mathbf{q}}$ contain the nodal displacements and accelerations, respectively, while in the column array $\mathbf{F}(t)$, the time histories of external nodal forces are assembled. The global matrices $\mathbf{M}, \mathbf{K}$ are assembled of local element mass and stiffness matrices that are expressed by

$$\mathbf{M}_\mathrm{e} = \int_{V_\mathrm{e}} \rho \mathbf{H}^\mathrm{T}\mathbf{H}\,\mathrm{d}V_\mathrm{e} \tag{20}$$

and

$$\mathbf{K}_\mathrm{e} = \int_{V_\mathrm{e}} \mathbf{B}^\mathrm{T}\mathbf{C}\mathbf{B}\,\mathrm{d}V_\mathrm{e}, \tag{21}$$

where ρ is the density, the matrix $\mathbf{H}$ stores the displacement interpolation functions (shape functions) and $\mathbf{B}$ is the strain-displacement matrix. The quadrature formulas defining the local mass and stiffness matrices are carried out within the element's undeformed volume V_e. In a plane strain problem of isotropic media, the elastic matrix $\mathbf{C}$ takes the form

$$\mathbf{C} = \frac{E}{(1+\mu)(1-2\mu)} \begin{bmatrix} 1-\mu & \mu & 0 \\ \mu & 1-\mu & 0 \\ 0 & 0 & \frac{1-2\mu}{2} \end{bmatrix}, \tag{22}$$

where E and μ are the Young's modulus and the Poisson's ratio, respectively. Usually, the standard full Gauss quadrature rule is employed for the evaluation of integrals (20), (21). The details of FE technology can be found in Hughes (2000) or Bathe (1996).

Commercial finite element packages offer a reduced quadrature process as well. This process, also called 'under-integration', increases efficiency and significantly reduces computational costs in nonlinear problems in wave propagation, as the data is stored in a limited number of integration points. One-point integration is commonly used for 1D, 2D and 3D linear finite element discretization in explicit time integration (Belytschko and Hughes 1983). In Mullen and Belytschko (1982), the dispersion of 2D finite elements with one-point integration of the stiffness matrix is studied for linear wave propagation, and it is shown that dispersion errors increase with this numerical approach. The under-integration of the mass matrix is not a common approach due to the loss of rank of the mass matrix and the influence on the rigid body modes (Felippa et al. 2015), and only the full integration is used for the mass matrix in real implementation. In elastic wave propagation, the full integration is used because the stiffness matrix is evaluated only once, making it a good candidate for minimizing dispersion errors. Selective and reduced integration are used for structural elements in statics to eliminate shear and volumetric locking.

Evaluating the equations of motion, prescribed by Eq. (19), by time marching operators, provides the *transient response* of a loaded body to generic loading, while applying the generalized eigenvalue problem to Eq. (19) with $\mathbf{F}(t) = 0$ gives the *steady-state response* of a body to harmonic excitations. In this paper, both approaches are used to study the temporal and spatial dispersion effects.

The element mass matrix, as well as the global mass matrix, is called consistent when derived 'consistently' using Eq. (20). Consistent mass matrices are recommended to be used with implicit time integration operators.

Diagonal (lumped) mass matrices minimize the computer storage requirements; furthermore, the inversion is trivial. Diagonal mass matrices are recommended to be used with explicit time integration operators (see Bathe 1996). To create a diagonal mass matrix, the so-called row-sum method is sometimes used. Such a process is suitable for linear elements only (see Hughes 2000; Belytschko et al. 2000). Unfortunately, the row-sum method, applied to mass matrices of higher-order elements, produces certain negative diagonal elements in the lumped matrices; furthermore, the lumped mass matrix does not satisfy positive definiteness. Note that the total mass of the lumped mass is fully conserved. That is why the diagonal mass scaling method, the so-called HRZ (Hinton–Rock–Zienkiewicz) method is preferred for the higher-order FEM and structural elements, such as beams, plates and shells (see Hinton et al. 1976). To conserve the overall mass and make a lump mass matrix positive definite, the diagonal elements should be properly scaled (see Felippa et al. 2015).

4. TIME INTEGRATION OF EQUATIONS DESCRIBING WAVE PROPAGATION IN ELASTIC SOLIDS

Stress wave propagation tasks in the elastic continuum are described by partial differential equations. For the prescribed boundary and initial conditions, the equations are difficult to solve analytically. The results are available for uncomplicated geometries and simple loading effects only. Solution procedures are often based on applying Fourier and Laplace transforms to the equations of motion, followed by inverse transforms, which leads to the outcome in the form of infinite series of integrals with infinity as their limit (Červ et al. 2016).

Using the finite element method in dynamics, discretization in space has to be complemented by **discretization in time** when treating wave propagation tasks since time variable and, consequently, inertia effects have to be considered. By time discretization, partial differential equations of motion – typical for the solid continuum – are replaced by ordinary differential equations.

Their numerical solutions can be obtained by mode superposition and direct integration methods (see Bathe 1996). Here, the latter methods will be treated.

We will focus our attention on the numerical approaches specific to the time discretization of ordinary differential equations that describe transient wave propagation tasks in solids, modelled using the displacement version of the finite element method.

Elastic waves, modelled by finite element methods, are described by equations of motion in the form of a system of second-order ordinary linear differential equations

$$\mathbf{M}\ddot{\mathbf{q}} + \mathbf{D}\dot{\mathbf{q}} + \mathbf{K}\mathbf{q} = \mathbf{F}(t), \tag{23}$$

where $\mathbf{M}, \mathbf{D}, \mathbf{K}$ are the global mass, viscous damping and stiffness matrices, respectively; $\ddot{\mathbf{q}}, \dot{\mathbf{q}}, \mathbf{q}$ are column arrays of kinematic variables, i.e. generalized accelerations, velocities and displacements at nodes; and $\mathbf{F}(t)$ is the array of external nodal loading forces expressed as functions of time. An example of modelling damping effects is the classical Rayleigh damping matrix (see Chopra 2001), as

$$\mathbf{D} = \mu_1 \mathbf{M} + \mu_2 \mathbf{K}, \tag{24}$$

where μ_1 and μ_2 are the Rayleigh damping coefficients, respectively, often determined by the vibration experiments of structures. Time integration methods give histories of kinematic variables, and, subsequently, using the infinitesimal Cauchy relations, the strain quantities are evaluated. Finally, the stress quantities are obtained using linear constitutive relations (see Bathe 1996; Park 1977; Park et al. 2012; Zienkiewicz 1971).

The aim of computational procedures used for the solution of transient problems is to satisfy the equations of motion, not continually but rather at discrete time intervals. It is assumed that all kinematic quantities for times $0, \Delta t, 2\Delta t, 3\Delta t \ldots t$ are known, while those for times $t + \Delta t \ldots t_{\max}$ are to be found. The quantity Δt, called the timestep size, does not necessarily need to be constant throughout the integration process.

Time integration methods can be broadly characterized as explicit (see Dokainish and Subbaraj 1989), or implicit (see Subbaraj and Dokainish 1989).

4.1. Explicit time integration algorithms

Explicit formulations stem from equations of motion written at time t. This is indicated by an upper right index. As we said, the discretized equations of motion in FEM have the form at each time t as

$$\mathbf{M}^t\ddot{\mathbf{q}}^t + \mathbf{D}^t\dot{\mathbf{q}}^t + \mathbf{K}^t\mathbf{q}^t = \mathbf{F}(t). \tag{25}$$

If the transient problem is linear, and we assume elastic wave propagation, then the mass, damping and stiffness matrices do not change in time. A classical representative of the explicit time integration algorithm is the central difference scheme. Substituting the central difference approximations for velocities and accelerations

$$\dot{\mathbf{q}}^t = \left(\mathbf{q}^{t+\Delta t} - \mathbf{q}^{t-\Delta t}\right)/(2\Delta t), \tag{26}$$

$$\ddot{\mathbf{q}}^t = \left(\mathbf{q}^{t+\Delta t} - 2\mathbf{q}^t + \mathbf{q}^{t-\Delta t}\right)/(\Delta t)^2 \tag{27}$$

into equations of motion (25) gives us a system of algebraic equations that we can solve for the displacements at time $t+\Delta t$, namely

$$\mathbf{M}^{\text{eff}}\mathbf{q}^{t+\Delta t} = \mathbf{F}^{\text{eff}}, \tag{28}$$

where the so-called effective quantities are

$$\mathbf{M}^{\text{eff}} = \mathbf{M}/(\Delta t)^2 + \mathbf{D}/(2\Delta t) \tag{29}$$

and

$$\mathbf{F}^{\text{eff}} = \mathbf{F}^t - \left(\mathbf{K} - 2\mathbf{M}/(\Delta t)^2\right)\mathbf{q}^t - \left(\mathbf{M}/\Delta t^2 - \mathbf{D}/(2\Delta t)\right)\mathbf{q}^{t-\Delta t}. \tag{30}$$

The last term in the above expression for effective force indicates that the process is not self starting. For more details, see Bathe (1996). The computational process can be written in the form of unknown accelerations (A-form) (see Hughes 2000) against the displacement form (D-form).

The process is, however, explicit only if the mass matrix is made diagonal by a suitable lumping process (Zienkiewicz 1971). The damping matrix needs to be diagonal as well. The inversion of $\mathbf{M}^{\text{eff}}$ is then trivial and, instead of solving the system of algebraic equations, we simply have the set of individual equations for each degree of freedom, and no matrix solver is actually needed. This makes the system of equations easy to parallelize.

A comprehensive survey of explicit time integration methods for dynamic analysis of linear and nonlinear structures can be found in Dokainish and Subbaraj (1989). A thorough analysis of transient algorithms together with a rich source of references was presented in the book by Belytschko and Mullen (1978). Stability analyses of explicit and implicit schemes has been studied for a long time. Park (1977) has investigated stability limits and stability regions for both linear and non-linear systems. A comprehensive survey showing a variety of approaches is presented in the book by Hughes and Liu (1978).

The explicit methods are only conditionally stable; the stability limit being approximately equal to the time for an elastic wave to traverse the smallest element. The critical timestep securing the stability of the central difference method for a linear undamped system is $\Delta t_{\text{crit}} = 2/\omega_{\max}$ (see Lew et al. 2004), $\omega_{\max}$ being the maximum eigenfrequency, related to the maximum eigenvalue $\lambda_{\max}$ of the generalized eigenvalue problem $\mathbf{Kq} = \lambda\mathbf{Mq}$ by $\omega^2 = \lambda$. Practical calculations show that the result is also applicable to nonlinear cases since each timestep in the nonlinear response can roughly be considered as a linear increment of the whole solution.

Often, the critical timestep size Δt_{crit} is related to the characteristic length of the finite element H_{char} and the corresponding maximum elastic wave speed in the media $c_{\max}$ as $\Delta t \leq \Delta t_{\text{crit}} = \alpha\frac{H_{\text{char}}}{c_{\max}}$, the parameter α

depending on the finite element type, order of shape function, numerical integration, mass matrix, etc. For example, for a 1D case, the linear bar element with full integration and lumped mass matrix is given an α parameter of $\alpha = 1$. We can also define the Courant number – dimensionless timestep size – $C = \frac{\Delta t c_{\max}}{H_{\text{char}}}$.

Efficient and stable timestep estimation is to be included in the numerical process for modelling wave propagation in solids (see Park 1977). The estimated value of Δt should be close to the critical value of the timestep size. In real FE explicit computations and commercial software, automated timestep estimation is employed as the power iteration method (Benson 1998) and as the Gershgorin circle-based timestep estimation (Kulak 1989).

The power iteration method is based on an iterative process for computing the maximum eigenvalue $\lambda_{\max}$ of the generalized eigenvalue problem $\lambda \psi_{n+1} = \mathbf{A}\psi_{\mathbf{n}}$ with $\mathbf{A} = \mathbf{M}^{-1}\mathbf{K}$ as the following procedure:

1. Initialize eigenvector ψ_0, e.g. random in range $[-1, 1]$, $i = 0$
2. $i = i + 1$
3. Compute $\psi_{i+1} = \mathbf{K}\psi_i$
4. Compute $\chi_{i+1} = \mathbf{M}^{-1}\psi_{i+1}$
5. Compute the estimate of eigenvalue $\lambda_{i+1}^{\max} = \|\chi_{i+1}\|$
6. Update eigenvector $\psi_{i+1} = \chi_{i+1}/\lambda_{i+1}^{\max}$
7. If $|\lambda_{i+1}^{\max}/\lambda_i^{\max} - 1| > \varepsilon$ or $i < N^{\text{iter}}$, go to STEP 2
8. $\lambda^{\max} = \lambda_{i+1}^{\max}$
9. $\omega_{\max} = \sqrt{\lambda^{\max}}$
10. $\Delta t_{\text{crit}} = 2/\omega_{\max}$

Practically, the process converges in several (e.g. 10) iterations. This estimation should include the effect of boundary conditions and composite meshes consisting of different finite element types. Practically, the final timestep for computation is taken to be $\Delta t = 0.9\Delta t_{\text{crit}}$ (see Hallquist 2006).

The other estimation of the stable timestep size is based on the Gershgorin circle theorem (Gershgorin 1931), where by applying the linear eigenvalue problem with the lumped mass matrix one can estimate the stable timestep size (Kulak 1989) as

$$(\omega_{\max})^2 \leq \max_i \frac{\sum_{j=1}^{n} |K_{ij}|}{M_{ii}}, \qquad \Delta t_{\text{crit}} = \frac{2}{\omega_{\max}}. \tag{31}$$

One can also use the Fried's theorem, which takes into account the element eigenvalue inequality $\omega_{\max} \leq \max_i \omega_i^e$ over all finite elements (Fried 1972).

Explicit time integration methods are employed mostly for the solution of nonlinear problems since implementing complex physical phenomena and constitutive equations is then relatively easy. The global mass matrix need not be assembled, and thus no matrix solver is required, which saves computer storage and time. The main disadvantage is the conditional stability, which clearly manifests itself in linear problems where the solution quickly blows up if the timestep is larger than the critical one. In nonlinear problems, results calculated with a 'wrong' step could contain a significant error and may not show immediate instability.

4.2. Implicit time integration algorithms

Implicit formulations stem from equations of motion written at time $t + \Delta t$; unknown quantities are implicitly embedded in the formulation, and the system of algebraic equations must be solved to 'free' them. In structural dynamic problems, implicit integration schemes give acceptable solutions with timesteps usually one or two orders of magnitude larger than the stability limit of explicit methods.

Perhaps the most frequently used implicit methods belong to the so-called Newmark family (Newmark 1959). The Newmark integration scheme is based upon an extension of the linear acceleration method in which it is assumed that the accelerations vary linearly within a timestep.

For linear transient tasks treated by the finite element method, the classical Newmark method consists of the following equations (see Newmark 1959):

$$\mathbf{M}\ddot{\mathbf{q}}^{t+\Delta t} + \mathbf{D}\dot{\mathbf{q}}^{t+\Delta t} + \mathbf{K}\mathbf{q}^{t+\Delta t} = \mathbf{F}^{t+\Delta t}, \tag{32}$$

$$\mathbf{q}^{t+\Delta t} = \mathbf{q}^t + \Delta t\dot{\mathbf{q}}^t + \frac{1}{2}(\Delta t)^2\left((1-2\beta)\ddot{\mathbf{q}}^t + 2\beta\ddot{\mathbf{q}}^{t+\Delta t}\right), \tag{33}$$

$$\dot{\mathbf{q}}^{t+\Delta t} = \dot{\mathbf{q}}^t + \Delta t\left((1-\gamma)\ddot{\mathbf{q}}^t + 2\gamma\ddot{\mathbf{q}}^{t+\Delta t}\right). \tag{34}$$

Equations (32) to (34) suffice for the determination of three unknowns, i.e. $\mathbf{q}^{t+\Delta t}$, $\dot{\mathbf{q}}^{t+\Delta t}$ and $\ddot{\mathbf{q}}^{t+\Delta t}$. The parameters β and γ determine the stability and accuracy of the algorithm and were initially proposed by Newmark as $\beta = 1/4$ and $\gamma = 1/2$, thus securing the unconditional stability of the method, which means that the solution, for any set of initial conditions, does not grow without bounds regardless of the timestep. However, unconditional stability itself does not guarantee accurate and physically sound results (see Belytschko and Hughes 1983; Park 1977; Subbaraj and Dokainish 1989; Goudreau and Taylor 1973).

With the values of $\beta = 1/4, \gamma = 1/2$, the method is sometimes referred to as the constant-average acceleration version of the Newmark method and is widely used for structural dynamic problems. In this case, the method conserves energy. For linear problems, the mass, damping and stiffness matrices are constant, and the method leads to the repeated solution of the system of linear algebraic equations at each timestep, giving the displacements at time $t + \Delta t$ by solving the system

$$\mathbf{K}^{\text{eff}}\mathbf{q}^{t+\Delta t} = \mathbf{F}^{\text{eff}}, \tag{35}$$

where the so-called effective quantities are

$$\mathbf{K}^{\text{eff}} = \mathbf{K} + a_1\mathbf{M} + a_{1\text{d}}\mathbf{D}, \tag{36}$$

$$\mathbf{F}^{\text{eff}} = \mathbf{F}^{t+\Delta t} + \mathbf{M}(a_1\mathbf{q}^t + a_2\dot{\mathbf{q}}^t + a_3\ddot{\mathbf{q}}^t) + \mathbf{D}(a_{1\text{d}}\mathbf{q}^t + a_{2\text{d}}\,\dot{\mathbf{q}}^t + a_{3\text{d}}\ddot{\mathbf{q}}^t). \tag{37}$$

New accelerations and velocities are

$$\ddot{\mathbf{q}}^{t+\Delta t} = a_1(\mathbf{q}^{t+\Delta t} - \mathbf{q}^t) - a_2\dot{\mathbf{q}}^t - a_3\ddot{\mathbf{q}}^t \tag{38}$$

and

$$\dot{\mathbf{q}}^{t+\Delta t} = \mathbf{q}^t + a_4\ddot{\mathbf{q}}^t + a_5\ddot{\mathbf{q}}^{t+\Delta t}. \tag{39}$$

The constants are given as follows:

$$\begin{aligned} &a_1 = 1/\left(\beta(\Delta t)^2\right),\ a_2 = 1/\left(\beta(\Delta t)\right),\ a_3 = 1/(2\beta) - 1,\\ &a_4 = (1-\gamma)(\Delta t),\ a_5 = \gamma(\Delta t),\\ &a_{1\text{d}} = \gamma/(\beta(\Delta t)),\ a_{2\text{d}} = \gamma/\beta - 1,\ a_{3\text{d}} = \tfrac{1}{2}(\Delta t)\left(\frac{\gamma}{\beta} - 2\right). \end{aligned} \tag{40}$$

An efficient implementation of the Newmark method for linear problems requires that direct methods (e.g. the Gauss elimination) are used for the solution of the system of algebraic equations. The effective stiffness matrix is positive definite, which allows one to proceed without a search for the maximum pivot. Furthermore, the effective stiffness matrix does not change in time and thus can be factorized only once, before the actual time marching. Thus, at each step, only factorization of the right-hand side and backward substitution is carried out. This makes the Newmark method very efficient; treating a problem with a consistent mass matrix requires even fewer floating point operations than using the central difference method.

The Newmark method has many practically applicable features. If $\gamma \geq \frac{1}{2}$ and $\beta = \frac{1}{4}\left(\frac{1}{2} + \gamma\right)^2$, the method is still unconditionally stable, but a positive algorithmic damping is introduced into the process. With $\gamma < \frac{1}{2}$, a negative damping is introduced, which eventually leads to an unbounded response. By varying the

values of parameters β and γ, the Newmark scheme describes a whole series of time integration methods – sometimes called the Newmark family.

If, for example, $\beta = 1/12$ and $\gamma = 1/2$, we get a well-known Fox–Goodwin formula, which is implicit and conditionally stable, else if $\gamma = 1/2$ and $\beta = 0$, then the Newmark method becomes a central difference method, which is conditionally stable and explicit (if mass and damping matrices are diagonal).

The *algorithmic damping*, introduced into the Newmark method by setting the parameter $\gamma > 1/2$ and calculating the other parameter as $\beta = \frac{1}{4}\left(\frac{1}{2} + \gamma\right)^2$, is frequently used in practical computations since it filters out the high-frequency components of the mechanical system response. This damping is generally viewed as desirable. Since the high-frequency components are very often mere artifacts of the finite element modelling, they are consequences of the discrete nature of the finite element model and its dispersive properties (Goudreau and Taylor 1973).

It is known that algorithmic damping adversely influences the lower modes in the solution as well. To compensate for the negative influence of algorithmic damping on the lower modes of behaviour, a modified Newmark method is used to ensure adequate dissipation in the higher modes, whilst simultaneously guaranteeing that the lower modes are not affected too strongly (see Stein et al. 2017; Hilber et al. 1977). Nowadays, a commonly used time integration method with controlled dissipation effects is the *generalized-α* method (see Chung and Hulbert 1993).

Notes

For conditionally stable methods (e.g. the method of central differences), the timestep must be $\Delta t \leq \Delta t_{\text{crit}}$. If it is not, these methods explode numerically.

For unconditionally stable methods (e.g. the constant-average acceleration version of the Newmark method), any timestep could theoretically be employed. But if $\Delta t \gg \Delta t_{\text{crit}}$, the integration method marches too fast in time to see the minute details of the vibration process, and, consequently, the high-frequency components of the propagating signal are not registered – they are filtered out of the numerical integration.

5. DISPERSION

5.1. History of dispersion

The history of dispersion goes back to our forefathers, such as Newton, Fourier, Brillouin, Kolsky, Brepta, Bažant, etc. (Brillouin 1953; Kolsky 1953; Brepta and Okrouhlík 1986; Stade 2005; Bažant and Celep 1982). In this respect, a one-dimensional homogeneous lattice, consisting of mass particles connected by massless springs, depicted in Fig. 1, should be recalled as the simplest example of dispersive media.

Isaac Newton (1642–1726) employed the homogeneous lattice model (all particles have the same mass and all the spring stiffnesses are identical) for the estimation of the speed of sound in the air, using the formula

$$c = d\sqrt{\frac{k}{m}} = \sqrt{\frac{kd}{\rho}} = \sqrt{\frac{E}{\rho}}, \tag{41}$$

where d is the distance between particles, k is the spring stiffness, m is the mass of the particle, and E is the Young modulus.

For the E variable he used the isothermal bulk modulus of air, which gave him a speed value smaller than that obtained experimentally. Later, in 1822, Laplace used the adiabatic bulk modulus, obtaining results in close agreement with reality.

Johann Bernoulli (1667–1748) in Basel and his son Daniel Bernoulli (1700–1782) in St. Petersburg showed independently that the lattice (see Fig. 1), composed of n mass particles, has n degrees of freedom and, consequently, n independent eigenfrequencies and eigenvectors.

Fig. 1. Mass particles connected by massless springs.

A thin rod of a constant cross-section, considered as a 1D elastic continuum, is a counterpart of the lattice. A thin rod, in contradistinction to the lattice, has an infinite number of degrees of freedom and frequencies. With only a little generalization, one might say that the lattice is a mental forerunner of the finite element method. The dispersion analysis presented in the paper is based on comparing the oscillatory responses of continuous and discretized bodies to an applied harmonic excitation. Figure 5 presents the dispersion relation between the frequency and the wave number for a lattice, as described in Brillouin (1953), and for a classical 1D constant finite strain element. The one mass-spring homogeneous lattice model and a thin bar modelled by a 1D constant finite strain element have the same dispersion relationship. The details of dispersion analysis will be explained later.

It was Euler (1748) who proved that the laterally vibrating string is formally described by the same type of partial differential equation as the longitudinally vibrating thin bar, i.e.

$$\frac{\partial^2 u}{\partial t^2} = c_0^2 \frac{\partial^2 u}{\partial x^2}. \tag{42}$$

In a vibrating spring, the variable u stands for lateral displacement, while for a vibrating lattice it represents longitudinal or axial displacements. Also, the definition of the constant c_0 is different. He also proved that the solution of the above equation (i.e. the distribution of displacements in space and time) could be assumed in the form $u(x,t) = f(x \pm c_0 t)$, where f is an arbitrary function satisfying certain continuity conditions (see Kolsky 1953). Such a solution is independent of the frequency of the propagating wave. In other words, in a 1D solid elastic continuum, the stress waves of all frequencies propagate at the same speed. So, a wave package composed of the whole spectrum of frequencies propagates within a thin rod forever, without any distortion. In this respect, the 1D solid continuum is considered to be a perfect *dispersionless* medium.

It is known that the dispersion side effects occurring due to discretization (actually, the flaws in the context of continuum modelling) cannot be fully eliminated. In this paper, we will reveal how to minimize them.

5.2. Types of dispersion

In solid continuum mechanics, we distinguish material, geometrical, spatial and temporal types of dispersion. *Material dispersion* is induced by the nonlinear elastic response and by the damping and microstructural properties of the medium through which the wave propagates. *Geometrical dispersion* occurs when one changes the geometrical shapes of waveguides through which the waves propagate. *Spatial discretization* of the continuum is typical for numerical approaches based on the process in which the originally continuum structure of the material is replaced by small finite parts – usually finite elements. Finally, *temporal discretization* – typical for the numerical solution of transient tasks – stems from the fact that the quantities resulting from the analytical solution of differential equations of motion, instead of being described by continuous functions of time, are evaluated in discrete time intervals only. In this text, only the spatial and temporal types of dispersion of FEM are discussed.

5.3. Spatial dispersion of FEM

Study of the spatial dispersion phenomena is based on assuming the harmonic wave, defined by its wave number and wave length, propagating in a specified direction. After that, this prescribed motion in time and

space is inserted into the equations of motion of a characteristic stencil of the problem to solve. Finally, the relationship between the angular velocity ω, the wave number k^h defined for a discrete model and the direction of wave propagation θ is found in a closed form as $\omega = f(k^h, \theta)$ or evaluated numerically. The vector of the numerical phase speed $\mathbf{c}^h$ is then computed via the relationship

$$\mathbf{c}^h = \frac{\omega}{\mathbf{k}^h} = \left(\frac{\omega}{k_x^h}, \frac{\omega}{k_y^h}, \frac{\omega}{k_z^h} \right), \tag{43}$$

and the vector of the numerical group velocity $\mathbf{c}_\mathrm{g}$ is defined as

$$\mathbf{c}_\mathrm{g}^h = \frac{\mathrm{d}\omega}{\mathrm{d}\mathbf{k}^h} = \left(\frac{\partial\omega}{\partial k_x^h}, \frac{\partial\omega}{\partial k_y^h}, \frac{\partial\omega}{\partial k_z^h} \right). \tag{44}$$

Note that the numerical wave speed $\mathbf{c}^h$, the numerical group speed $\mathbf{c}_\mathrm{g}^h$ and the wave number k^h defined for a discrete model are counterparts to the wave speed c, the group speed $\mathbf{c}_\mathrm{g}$ and the wave number k corresponding to the analytical results of wave propagation in elastic solids.

5.3.1. Constant strain 1D finite element

The simplest rod/bar finite element with two degrees of freedom, identified by displacements q_1, q_2, depicted in Fig. 2, is based on the assumption of linear displacement distribution within its length, which leads to a constant distribution of strain within the element (see Bathe 1996).

The local mass and stiffness matrices for a constant strain element are

$$\mathbf{M}_e = \frac{\rho A l_0}{6} \mathbf{M}_\mathrm{c}^*, \; \mathbf{M}_\mathrm{c}^* = \begin{bmatrix} 2 & 1 \\ 1 & 2 \end{bmatrix}, \tag{45}$$

$$\mathbf{K}_e = \frac{EA}{l_0} \mathbf{K}^*, \; \mathbf{K}^* = \begin{bmatrix} 1 & -1 \\ -1 & 1 \end{bmatrix}. \tag{46}$$

The non-dimensional part of the consistent mass matrix $\mathbf{M}_\mathrm{c}^*$ is alternatively considered in its diagonal form as

$$\mathbf{M}_\mathrm{d}^* = \begin{bmatrix} 3 & 0 \\ 0 & 3 \end{bmatrix}. \tag{47}$$

Constants A and l_0 are the cross-sectional area and length, while E and ρ are the Young's modulus and density, respectively.

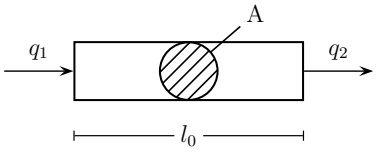

Fig. 2. Constant strain rod element.

The idea on which the dispersion study of an FE model is based is to introduce a harmonic wave propagation solution into a discrete system and observe what happens, and thus to determine the dispersion relationships (see Brillouin 1953; Okrouhlík and Höschl 1993). Imagine an infinitely long rod composed of identical constant strain elements. Assembling the global mass and stiffness matrices out of the local ones, we find that, in this case, the global mass and stiffness matrices $\mathbf{M},\mathbf{K}$ are of a tri-diagonal structure with a repeated pattern. A typical equation for the consistent mass matrix formulation, written in terms of the j-th node, is

$$\ddot{q}_{j-1}+4\ddot{q}_j+\ddot{q}_{j+1}-6\omega_0^2(q_{j-1}-2q_j+q_{j+1})=0, \tag{48}$$

where

$$\omega_0 = c_0/l_0. \tag{49}$$

Similarly, for the diagonal mass matrix formulation, we get

$$\ddot{q}_j+\omega_0^2(q_{j-1}-2q_j+q_{j+1})=0. \tag{50}$$

The dimensionless counterparts of wave length and wave number, related to the finite element length, are

$$\Lambda_0^h = \lambda^h/l_0 \ \ldots \text{ dimensionless wave length,}$$

$$\gamma^h = k^h l_0 = \frac{2\pi}{\Lambda_0^h} \ \ldots \text{ dimensionless wave number.}$$

$$\gamma^* = \frac{\gamma^h}{2\pi} = \frac{l_0}{\lambda^h} \ \ldots \text{ normalized dimensionless wave number.}$$

The Λ_0^h parameter determines how many element lengths, denoted by l_0, would fit into the wave length of a considered harmonic wave. In Fig. 3, we depict how the wave would look if Λ_0 were given a value of 6.

The numerical phase velocity is defined by

$$c^h = \frac{\omega}{k^h} = \frac{\lambda^h}{T} \ \text{[m/s]}.$$

The relative phase velocity, related to element length, is

$$w^h = \frac{c^h}{l_0} = \frac{\omega}{k^h}\frac{1}{l_0} = \frac{\omega}{\gamma^h} \ \text{[1/s]}.$$

A one-dimensional harmonic wave propagating in $\pm x$ direction can be expressed in the form

$$u(x,t) = Ce^{\mathrm{i}(k^h x \pm \omega t)};$$

for details, see Kolsky (1953). If x coordinate is discretized, i.e. $x_j = jl_0$, j being the node counter (see Fig. 4), then

$$q_j = Ce^{\mathrm{i}(k^h l_0 j \pm \omega t)} = Ce^{\mathrm{i}(\gamma^h j \pm \omega t)}.$$

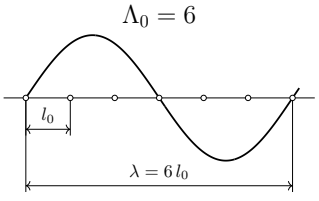

Fig. 3. Example of a wave with the dimensionless wave length $\Lambda_0 = \lambda/l_0 = 6$.

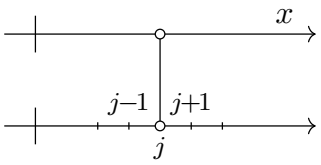

Fig. 4. Continuous and discretized quantities.

Considering the wave propagation with + sign only, we have

$$q_j = Ce^{\mathrm{i}(\gamma^h j+\omega t)} = Ce^{\mathrm{i}\gamma^h\left(j+\frac{\omega}{\gamma^h}t\right)} = Ce^{\mathrm{i}\gamma^h(j+w^h t)}. \tag{51}$$

Expressing the previous relation for the indices $j-1$, j and $j+1$, evaluating their second time derivatives and substituting them into Eq. (48), we get (the details are in Okrouhlík 2013)

$$\underbrace{\left(\gamma^{h2}w^{h2}+6\omega_0^2\right)}_{a}z^2+\underbrace{\left(4\gamma^{h2}w^{h2}-12\omega_0^2\right)}_{b}z+\underbrace{\left(\gamma^{h2}w^{h2}+6\omega_0^2\right)}_{a}=0, \tag{52}$$

a quadratic equation in terms of $z=e^{\mathrm{i}\gamma^h}$. Introducing a,b as indicated above, we have $az^2+bz+a=0$, whose roots are $z_{1,2}=\frac{-b\pm\sqrt{b^2-4a^2}}{2a}$.

Taking $b^2-4a^2<0$, i.e. $\omega=\gamma^h w^h<\omega_l^c=\sqrt{12}\omega_0$, to get the expected imaginary (i.e. vibrating) solution, and realizing that $z=e^{\mathrm{i}\gamma^h}=\cos\gamma^h+\mathrm{i}\sin\gamma^h$, we obtain $\cos\gamma^h=-\frac{b}{2a}$ and $\sin\gamma^h=\frac{\sqrt{4a^2-b^2}}{2a}$, and, finally

$$\left(6\omega_0^2+\gamma^{h2}w^{h2}\right)\cos\gamma^h=6\omega_0^2-2\gamma^{h2}w^{h2}. \tag{53}$$

The angular velocities for the consistent mass matrix formulation (indicated by c and d indices) are then evaluated:

$$\omega_c^*=\frac{\omega_c}{\omega_0}=\frac{w^h\gamma^h}{\omega_0}=\sqrt{\frac{6(1-\cos\gamma^h)}{2+\cos\gamma^h}}\qquad \gamma^h<0,\pi>, \tag{54}$$

with the phase speed related to c_0:

$$c_c^{*h}=\frac{c_c^h}{c_0}=\frac{1}{\gamma^h}\frac{\omega_c}{\omega_0}=\frac{1}{\gamma^h}\sqrt{\frac{6(1-\cos\gamma^h)}{2+\cos\gamma^h}}. \tag{55}$$

Similarly, the dispersion relation for the diagonal mass matrix is obtained in the form

$$\omega_d^*=\frac{\omega_d}{\omega_0}=\sqrt{2(1-\cos\gamma^h)}\qquad \gamma^h<0,\pi>, \tag{56}$$

with the phase speed related to c_0:

$$c_d^*=\frac{c_d^h}{c_0}=\frac{1}{\gamma^h}\sqrt{2(1-\cos\gamma^h)}\qquad \gamma^h<0,\pi>. \tag{57}$$

The frequency limit for the diagonal mass matrix is given as $\omega_l^d=2\omega_0$.

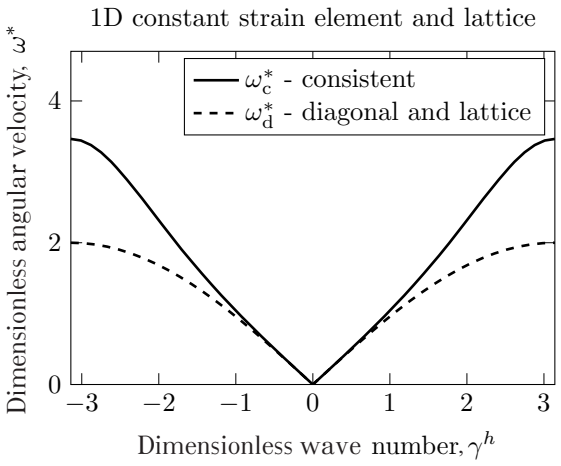

Fig. 5. Dispersion curves for a rod/bar assembled by 1D constant strain elements.

Figure 5 expresses the dispersion relation between the angular velocity ω^* and the wave number γ^h for a classical 1D constant strain element (see Okrouhlík and Höschl 1993). It is of interest that the dispersion curve, plotted by the dashed line and denoted by ω_d^*, stands for the 1D constant strain element with a diagonal mass matrix, while the solid line, denoted by ω_c^*, represents the dispersive behaviour of the constant strain element with a consistent mass matrix. More details can be found in Okrouhlík (2013).

The range of γ^h variable is $\langle 0, \pi \rangle$. If $\gamma_l^h = \pi$ ($l - limit$ value), then from $\gamma_l^h = \frac{2\pi}{\Lambda_{0l}}$ we get an important limit value

$$\Lambda_{0l} = 2. \tag{58}$$

This is the minimum limit value to ensure an FE response of vibrating character, meaning that at least two elements of the length l_0 should fit into the wave length λ of the considered harmonics, i.e. $\lambda_l^h = \Lambda_{0l} l_0 = 2l_0$. The wave propagation mode corresponds to a zig-zag tooth mode.

For larger values of ω than ω_l, the solution loses its vibrating character, and the attenuate wave mode is activated, with the corresponding wave length given by $\Lambda_{0l} = 2$, meaning two FEs fit the wave length. In this case, the waves are attenuated with respect to space, and the intensity of attenuation depends on the frequency of the propagating wave.

Figure 6 shows how the dimensionless phase velocity of a harmonic wave c^{*h} depends on the Λ_0 parameter. With an increasing number of elements, both relations (for consistent and diagonal mass matrices) approach the value '1', representing the ideal non-dispersive state. There are two parallel lines showing $\pm 1\%$ levels with respect to a phase velocity of one. The figure shows that for the dispersion error not to fall outside the $\pm 1\%$ limits, at least 13 element lengths should fit into the wave length of a harmonic wave – regardless of the mass matrix formulation. This rule of thumb is often generalized for other types of elements. Bathe (1996) recommends 10 element lengths; Okrouhlík and Pták (2005) frequently use the value 5. Dispersion analyses for other types of FEs are discussed in subsequent parts of this paper.

The results, as analytically derived formulas (54) and (56) for the assumption of the wave solution, can be compared with those acquired numerically by solving the generalized eigenvalue problem using global stiffness and mass matrices. In our case, we have the eigenvalue problem in the form

$$(\mathbf{K} - \omega^2 \mathbf{M})\,\mathbf{q} = \mathbf{0}. \tag{59}$$

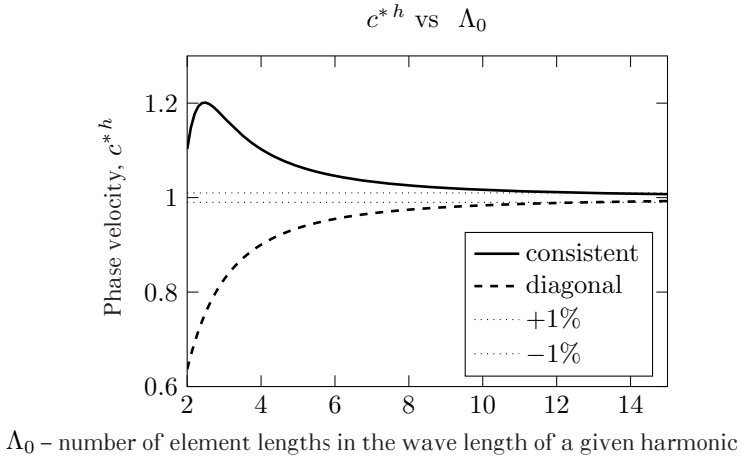

Fig. 6. Dimensionless phase velocity vs Λ_0 parameter.

The mathematical proof of equivalence between dispersion analysis and eigenvalue analysis for the 1D case has been published in the work of Hughes et al. (2008).

Figure 7 shows the results obtained analytically and numerically by the eigenvalue problem (59). The generalized eigenvalue problem was solved for a rod modelled by 30 constant strain elements with consistent (L1C) and diagonal (L1D) mass matrix formulations (L stands for the Lagrangian interpolation of displacements, number 1 stands for the first order polynomial, and C and D indicate consistent and diagonal mass matrix formulations, respectively). In this case, where both ends of the rod were considered free, the FE model has only 31 frequencies instead of an infinite number – typical for a 1D continuum. The dispersive relations presented in Fig. 7 are shown in three forms: angular velocity as a function of the counter of the degrees of freedom (1 to 31), phase velocity as a function of the counter and, finally, phase velocity vs angular velocity. The non-dispersive behaviour of a 1D continuum is shown as well. The most 'eloquent' is the subfigure in the lower part of Fig. 7, showing dispersive relations described by (54) and (56).

We shall summarize. The *1D continuum*, represented by the wave equation (42), is a non-dispersive medium with an infinite number of frequencies. The phase velocity of a propagating harmonic wave is constant, regardless of its frequency.

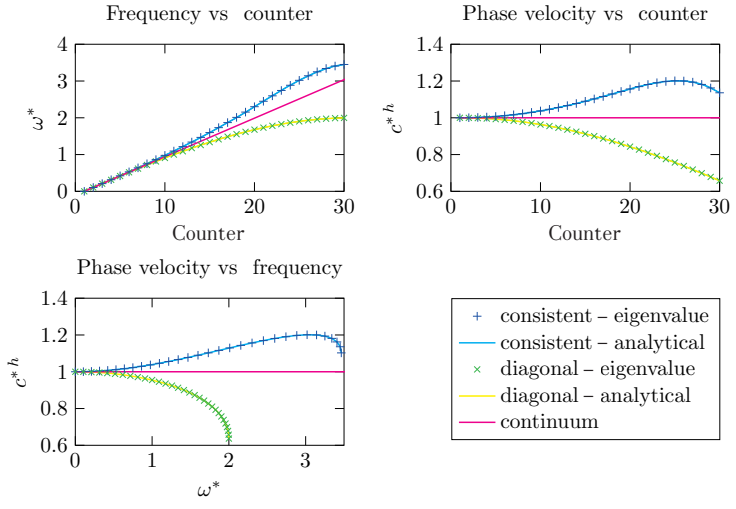

Fig. 7. Dispersive behaviour of 1D constant strain elements with consistent (L1C) and diagonal (L1D) mass matrix formulations.

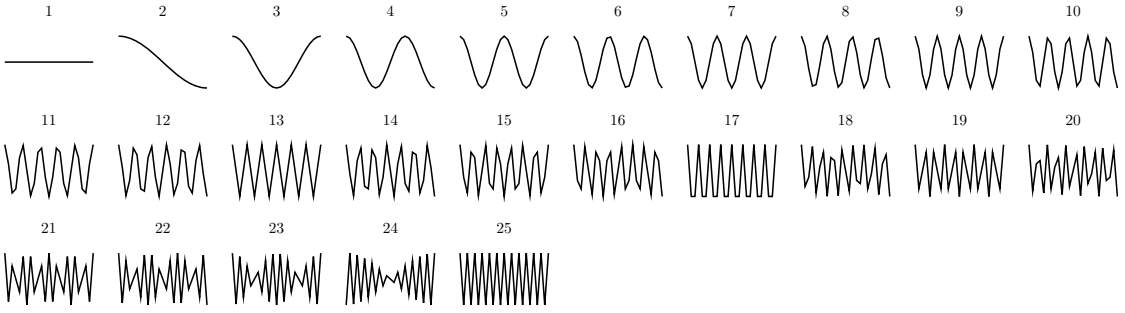

Fig. 8. All 25 axial eigenmodes of a thin rod modelled by 24 constant strain elements with a consistent mass matrix.

The *finite element model* is of dispersive nature. This means that it has a finite number of frequencies; the velocity of propagation depends on the frequency of a propagating harmonic wave, and, furthermore, the frequency spectrum is bounded. The limit frequency, corresponding to the limit value of the angular velocity ω_l, is called the *cut-off frequency*. In this respect, the finite element model of a continuum behaves as a *high-pass frequency filter*. The mechanical consequence of such a frequency limit is that in an FE model the harmonic waves with frequencies higher than that limit cannot be propagated. They are attenuated, which mathematically means that a propagating wave with a frequency higher than the cut-off frequency changes its harmonic vibrating character to an exponential decay form – an attenuated wave (see Brillouin 1953; Abboud and Pinsky 1992).

Besides the eigenfrequencies, the eigenmodes are also influenced by dispersion effects. Figure 8 presents the FE eigenmodes (modes of longitudinal vibration) computed numerically from Eq. (59), considering 24 constant strain elements. Since the frequencies correspond to the axial vibrations of the rod, the corresponding eigenmodes represent the axial modes of vibration. To show them in a meaningful way, they are plotted perpendicular to the axial axis. To emphasize – they do not represent the bending modes.

The first eigenmode, corresponding to the zeroth frequency – representing the case with no vibration at all – belongs to the zeroth frequency and to the corresponding rigid body motion of the rod, which (since both its ends are free of support) can freely move as a rigid body. According to the 1D continuum theory (Kolsky 1953), the following eigenmodes of a free-free thin rod are described by a cosine function in space. As far as the shapes of vibrating modes are concerned, the results of the finite element model for small frequencies agree relatively well with those of the idealized 1D continuum model. Higher modes, however, have 'wrong' shapes. By using more elements, we will have a higher number of 'correct' modes, but regardless of the number of elements used, the highest modes will not be represented correctly since the finite element model (composed of elements of finite size) is not as flexible as the ideal continuum, whose 'elements' are of infinitesimal dimensions. The highest continuum frequency, corresponding to a null-sized infinitesimal element, would have an infinitely high value. Evidently, for the higher frequencies, the FE model behaviour is not in accordance with an *a priori* assumed harmonic solution, which, as a shape function, was inserted into the equations of motion. And this is the dispersion.

Look at the last eigenmode, corresponding to the highest, in this case, the 25th frequency. We see that instead of the expected cosine displacement mode, we have a mode composed of straight lines connecting the neighbouring element nodes. This shows that these nodes vibrate in opposition. And since the constant strain element was born with a linear shape function for displacements, there is no way for a rod composed of these elements to vibrate more violently. This is a fine geometrical explanation of the limited highest frequency ω_l that can be transmitted through an FE model.

5.3.2. Higher-order 1D finite elements

The dispersion analysis of higher-order 1D elements (i.e. quadratic and cubic) (see Okrouhlík and Höschl 1993) reveals that by using these elements in 1D, we get a chance to increase the cut-off limit of the highest available frequency but at the expense of higher computing costs and the appearance of *bandpass filters*. The

dimensionless phase velocities as functions of dimensionless frequencies for 40 linear (L1)[1], 20 quadratic (L2) and 13 cubic (L3) finite elements[2] are depicted in Fig. 9. One can observe that for the higher-order elements, the first part of the dispersion curves, called the *optical branch*, is 'improved'. The dispersion diagrams, however, consist of distinct branches that are separated by certain frequency regions (called the *bandpass filters*) through which the particular frequencies cannot propagate. We say that the waves within these regions are *attenuated*[3], meaning that the mathematical description of waves changes pattern from harmonic to exponential.

For the L2 element, the second part of the dispersion function is called the *acoustic branch* (see Brillouin 1953). For the L3 element, there is the third part, which is traditionally also called the *optical branch*. The terminology was introduced by Brillouin (1953). In Fig. 9, the attributes C and D, appearing by the L1, L2 and L3 identifiers, signify the consistent and diagonal mass matrix formulations, respectively. In Fig. 10, all 40 eigenmodes of a bar consisting of 13 L3C FEs are depicted. There are longer 'dispersionless' parts both for speeds and for modes. The higher vibration modes are, however, hopelessly 'spoiled' (see Okrouhlík and Höschl 1993).

Okrouhlík and Höschl (1993) also present the analysis of the so-called Hermitian elements, which are based on the Hermitian interpolation in which not only displacements are approximated but also their first derivatives (strains) and the derivatives of those strains. The dispersion analysis of the B-spline based FE with a higher-order continuity over the FE boundary is described in the works of Kolman et al. (2014) and Kolman et al. (2017). Spline functions are used as testing and shape functions. In these works, dispersive behaviour has been studied with respect to the order of spline, order of continuity and type parametrization.

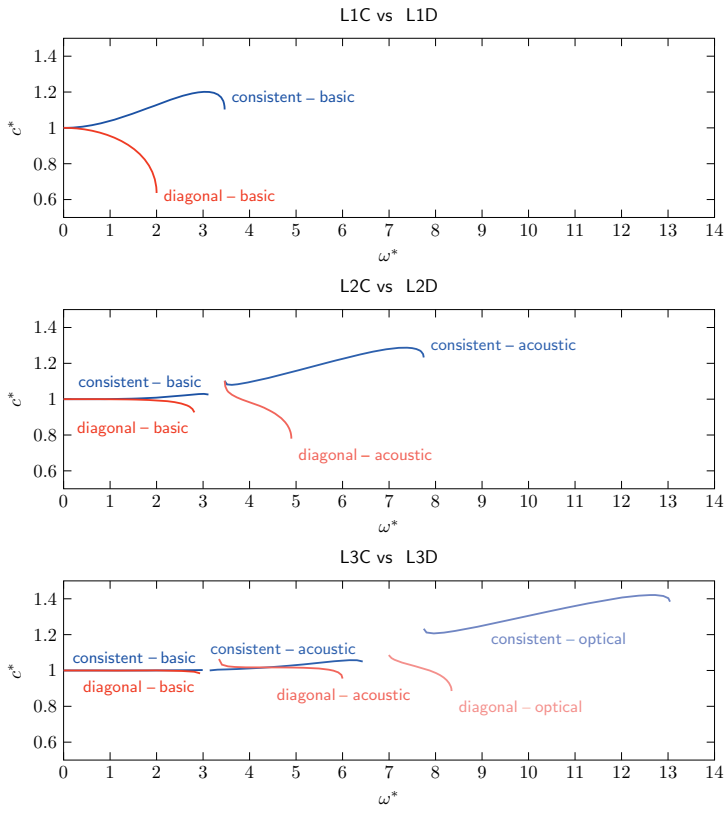

Fig. 9. Dispersion diagrams for L1, L2 and L3 elements.

[1] L stands for the Lagrangian approximation of displacements.

[2] The number of elements was chosen in such a way that the numerical effort for the evaluation of all three cases is roughly identical.

[3] Attenuation has nothing in common with damping. It is not accompanied with any loss of energy.

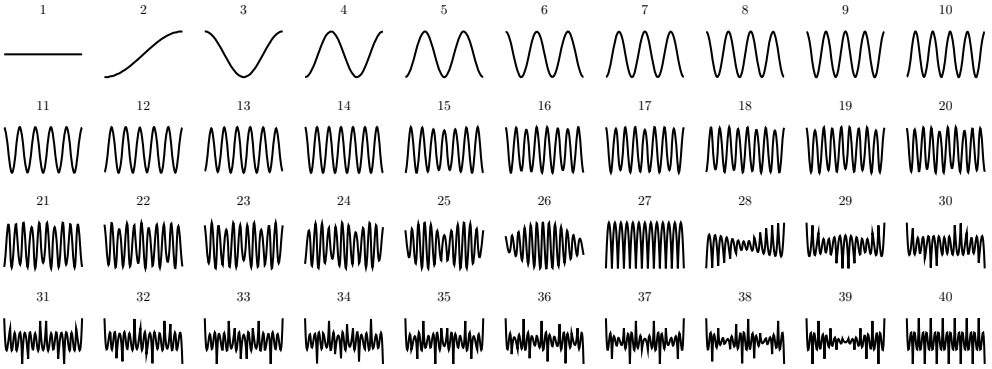

Fig. 10. Eigenmodes for L3C elements.

5.3.3. Linear 2D finite elements

The dispersion analysis of *equilateral triangle linear elements* has been studied in Brepta and Okrouhlík (1984) and bilinear (*4-node*) and biquadratic serendipity (*8-node*) finite elements in Kolman et al. (2016b). The dispersion graphs of the equilateral triangle linear elements are presented in Figs 11 and 12, dispersion diagrams of the bilinear FEs are presented in Fig. 13. As we have seen before, the elements with a consistent mass matrix (plotted by dashed lines) overestimate the 'correct' speed of propagation (horizontal lines), while the speed of propagation for elements with a diagonal mass matrix is systematically underestimated.

In the discretized 2D continuum, the speed of propagation is furthermore influenced by the direction of wave propagation. This means that a discretized 2D medium exhibits anisotropy behaviour, which does not exist in an ideal 2D isotropic elastic continuum. The *dispersion-induced anisotropy*, resulting from modelling stress wave propagation by equilateral triangle linear elements with consistent and lumped mass matrices, depicted in Fig. 12, is presented using velocity hodographs of wavefronts of waves emanating from the origin (polar diagram). Wave speeds are normalized with respect to the velocity of longitudinal waves, i.e. to c_1. The wavefronts for longitudinal as well as for shear waves are shown. Besides wavefronts for the 2D continuum (perfect circles), we see plotted the distributions for three ratios of λ^h (numerical wave length) to H (element size), as the parameter $\gamma^* = H/\lambda^h$. Again, short waves (relative to the mesh size) exhibit larger dispersion errors. For more details, see Brepta et al. (1985) and Brepta and Okrouhlík (1986).

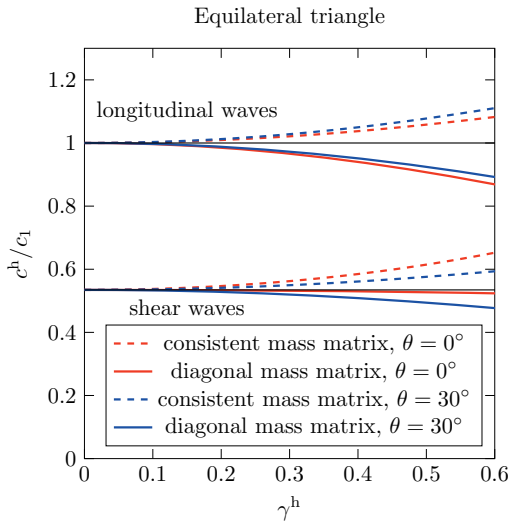

Fig. 11. Dispersion of 2D equilateral triangles under plain strain.

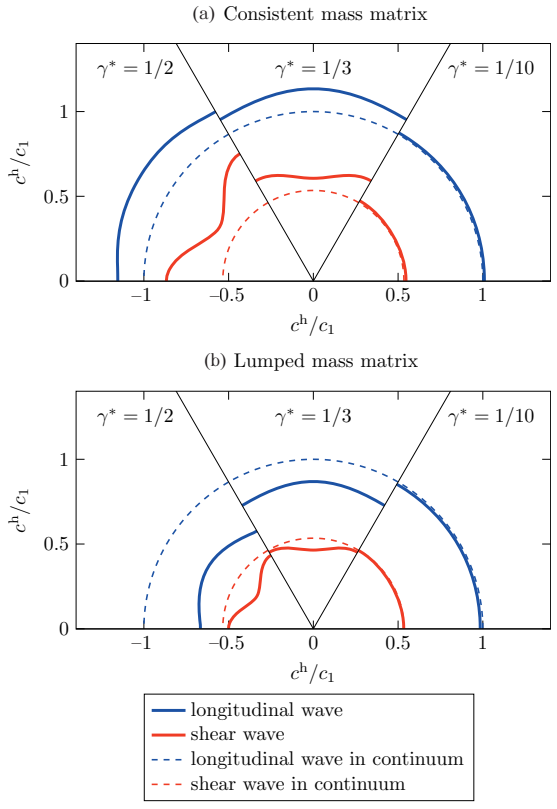

Fig. 12. Dispersion-induced anisotropy, shown by hodographs of wavefront velocities, for a 2D equilateral triangular finite element under plain strain with (a) consistent and (b) lumped mass matrices.

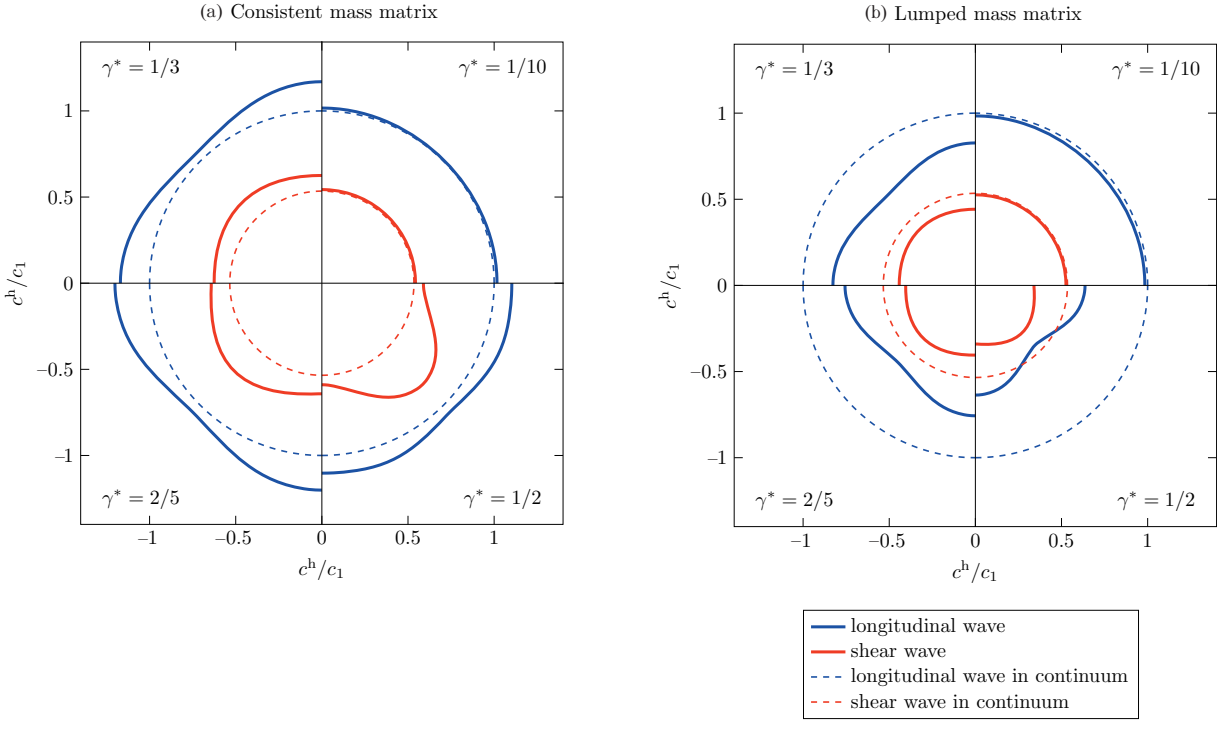

Fig. 13. Dispersion-induced anisotropy for a 4-node bilinear square element with (a) consistent and (b) lumped mass matrices.

The dispersive behaviour of a *4-node bilinear square finite element* with consistent and diagonal (lumped) mass matrices is worth recollecting. In Fig. 13, hodographs are presented, showing the positions of longitudinal and transversal wavefronts emanating from the origin, with the resultant dispersion-induced anisotropy. The wave speeds are normalized by the wave speed of the longitudinal wave, i.e. c_1. Four different ratios of mesh size to wave length are considered. For example, the ratio $\lambda^h = 10H$, (i.e. $\gamma^* = 1/10$) means that the wave length is just 1/10 of the mesh size. The effects of temporal dispersion due to different timestep operators are treated in detail in Section 6.

5.3.4. Higher-order 2D finite elements

Similar to higher-order 1D elements, the dispersion analysis of these 2D elements reveals that there are acoustic and optical branches appearing in the spectrum. Bandpass filters also appear in Kolman et al. (2013).

In Fig.14, we see the dispersion diagram for a wave that propagates in the direction of the x coordinate axis. Dimensionless wave speeds are plotted against dimensionless angular velocities. Figure 11 provides a comparison in which $\delta = 0$. It shows the situation for a 4-node bilinear square element in which there are two branches, one for a longitudinal and the other for a transversal wave. For further comparison, the dispersion diagram for an 8-node biquadratic square element is shown in Fig. 14. There are two acoustic branches (one for a longitudinal and one for a transversal wave) and four optical ones (two for a longitudinal and two for a transversal wave). The bandpass filter regions, where wave attenuation occurs, are plotted using dashed lines.

The analysis shows that the wave speeds in the optical mode range may reach infinite values even if the corresponding group velocities remain finite. The model of continuum based on 2D quadratic square elements exhibits unrealistic wave behaviour for optical modes. Also, the existence of bandpass filters, evoking wave attenuation, is seen – it is indicated by dashed lines.

The *dispersion-induced anisotropy* of an 8-node quadratic square element is shown in Fig. 15 for both consistent and diagonal mass matrices. The diagrams indicate that dispersion-induced anisotropy is more pronounced for shorter waves (higher frequencies), while propagation speeds are systematically smaller for diagonal mass matrix formulations. As before, the long waves (low frequencies) – for example, characterized by the ratio of the order of $\gamma^* = H/\lambda^h = 1/10$ – are subjected to smaller dispersion side effects.

Practical consequences of dispersion-induced attenuation effects are studied using a test involving numerical integration in time. This way, the test results – even if trying to minimize them – are additionally influenced by temporal discretization errors. Overall, spatial and temporal discretization effects will be discussed in the next paragraphs of this paper. For a fuller treatment, see Kolman et al. (2016b).

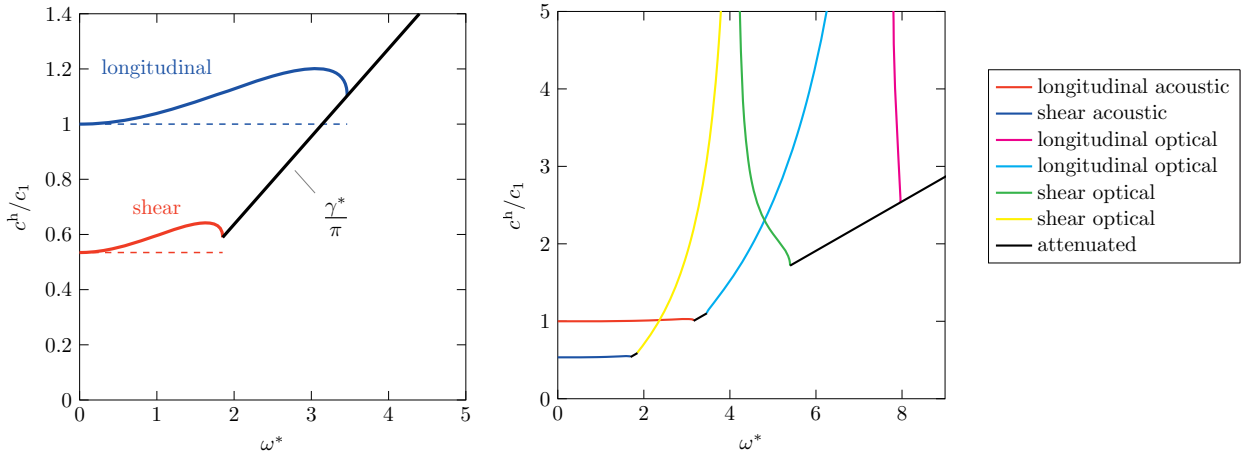

Fig. 14. Dispersion diagrams for linear 4-node and 8-node square elements.

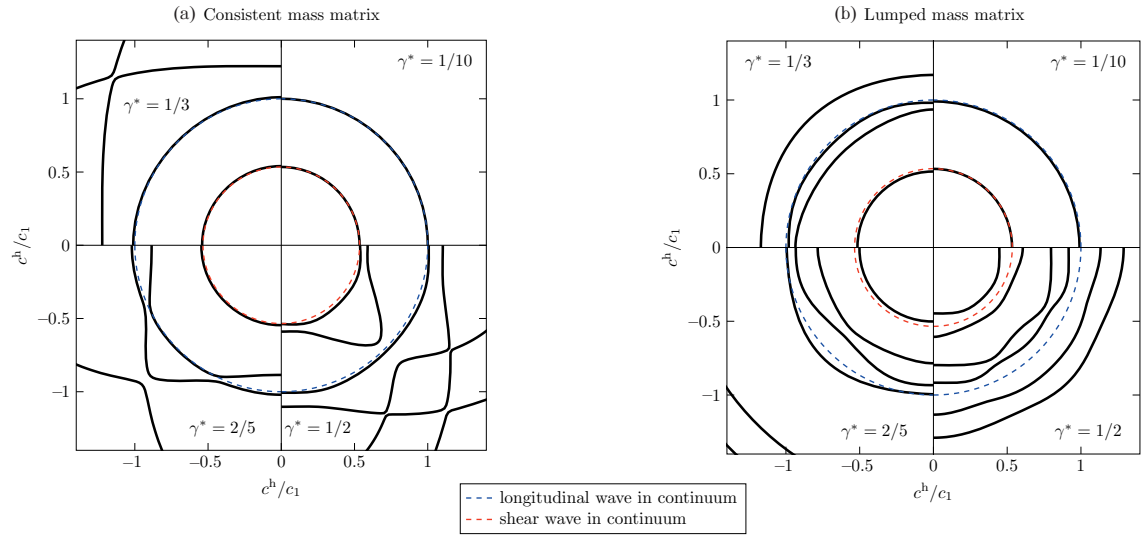

Fig. 15. Dispersion-induced anisotropy shown by hodographs of wavefront velocities. 8-node quadratic square element: (a) consistent and (b) diagonal mass matrix.

The following input data are used in the test: square planar geometry in the state of plane stress, assembled of 100×100 identical square 8-node biquadratic elements, each with the size of $H = 1$ mm. Elastic constants are: Young's modulus $E = 1$ MPa, Poisson's ratio $\mu = 0.3$ and density $\rho = 1\ \mathrm{kg/m^3}$. The corresponding wave speed is $c_1 = 1.16024\ \mathrm{m/s}$, while the ratio of speeds is $c_1/c_2 = 1.87083$.

The system is excited by a harmonic point force acting in the middle of the square planar geometry in the direction of the horizontal axis. The angular velocity range of the applied force is varied in such a way that it covers the whole spectrum of frequencies, as is depicted in Fig. 16.

The tested angular velocities (in dimensionless form, i.e. $\omega H/c_1 = \{1.0, 4.5, 7.9, 8.3\}$) are indicated by circles. The limits of individual dispersion branches are also presented. The attenuation regions are indicated by dashed lines. The time integration of governing equations of motion is provided by means of the Newmark method with no algorithmic damping, using the timestep $\Delta t = 1 \times 10^{-5}$s. This value of the timestep (expressed by the dimensionless Courant number $C = c_1 \Delta t/H = 0.011602$) is considered sufficiently small to minimize the effects of the temporal dispersion mentioned in Section 5.4.

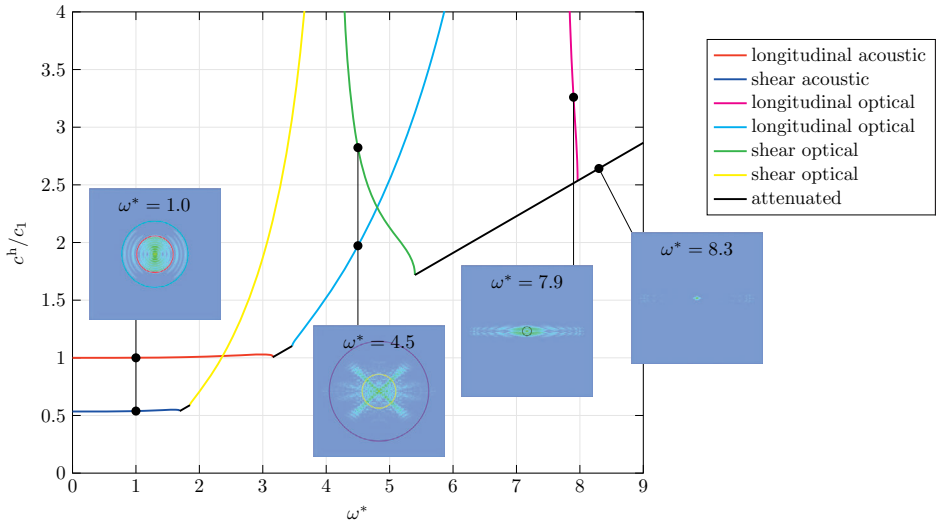

Fig. 16. Effects of attenuation for different dimensionless angular velocities.

Further dispersion curves are plotted in Fig. 16 – this time accompanied by numerical values indicating the ranges of individual branches. Displacement distributions (evaluated for a certain time value) are diagrammatically added, showing the prescribed excitations for four distinct dimensionless angular velocities, i.e. $\{1.0, 4.5, 7.9, 8.3\}$. Theoretical wavefronts for longitudinal and transversal waves are depicted as well. For frequencies within the acoustic mode region, the wavefronts are represented rather correctly. For the higher frequencies within the range of optical modes, one can observe the devastating effect of the attenuation phenomenon.

In practical engineering computations, we do not deal with propagation of monochromatic waves but with finite-length pulses of various shapes. And these, looking at them through the prism of the Fourier analysis (Stade 2005), are composed of an infinite number of harmonics whose frequency spectrum ranges from zero to infinity.

5.4. Temporal-spatial dispersion of FEM

Historically, the dispersion errors of spatial and temporal discretizations were treated independently. Today, both approaches are considered simultaneously to achieve reliable FE modelling of transient tasks in solid continuum mechanics. To limit discretization errors, one must not only minimize the timestep and the mesh size but also correctly relate the choice of the time integration operators with the mass matrix formulations. The situation is **schematically** depicted in Fig. 17, where temporal and spatial discretization errors – depending on the choice of time integration operators and mass matrix formulations – are plotted vs the timestep and the mesh size, respectively.

One sees that the temporal discretization errors of the central difference method (representing the explicit methods) and the spatial discretization errors of the diagonal mass matrix formulation produce errors of opposite signs, which have a tendency to cancel each other out. The same favourable situation exists for the Newmark method (representing the implicit methods) combined with a consistent mass matrix formulation. Two other combinations are clearly unsuitable (see Okrouhlík 1994).

The temporal-spatial dispersion polar diagram of the bilinear FEM for the explicit time integration with the diagonal mass matrix is shown in Fig. 18 (see Kolman et al. 2016b), and for the implicit time integration with the consistent mass matrix in Fig. 19 (see Kruisová et al. 2019). The results in Fig. 18 are presented for the 4-node bilinear element with a diagonal mass matrix for different mesh size to wave length ratios $\gamma^* = \{1/10, 1/3, 2/5, 1/2\}$ and for different Courant numbers $\{0, 0.5, 0.95, 1.0\}$. The zero Courant number is taken as a limit approach, and it corresponds to the spatial dispersion analysis. The results in Fig. 19 are presented for the 4-node bilinear element with a consistent mass matrix for different mesh size to wave length ratios $\gamma^* = \{1/10, 1/3, 2/5, 1/2\}$ and for different Courant numbers $\{0, 0.5, 1.0, 2.0\}$. It is of interest to compare the results presented in Fig. 13, which show the dispersion effects for the 4-node bilinear square element with consistent and lumped mass matrices, based on the spatial consideration only, with those in Figs 18 and 19, where both the temporal and spatial discretization effects are taken into account for the corresponding time integration type and mass matrix.

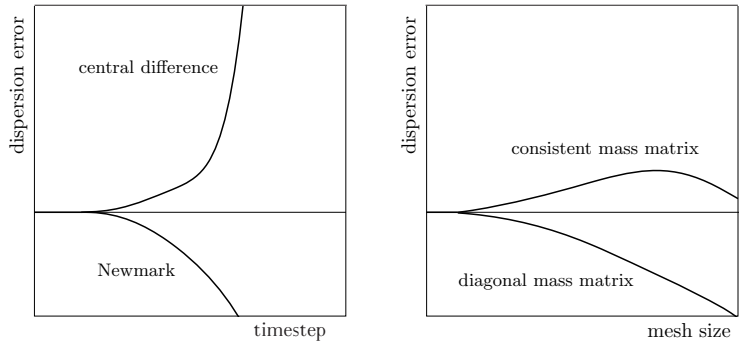

Fig. 17. Temporal and spatial discretization errors – influence of time integration operators and mass matrix formulations.

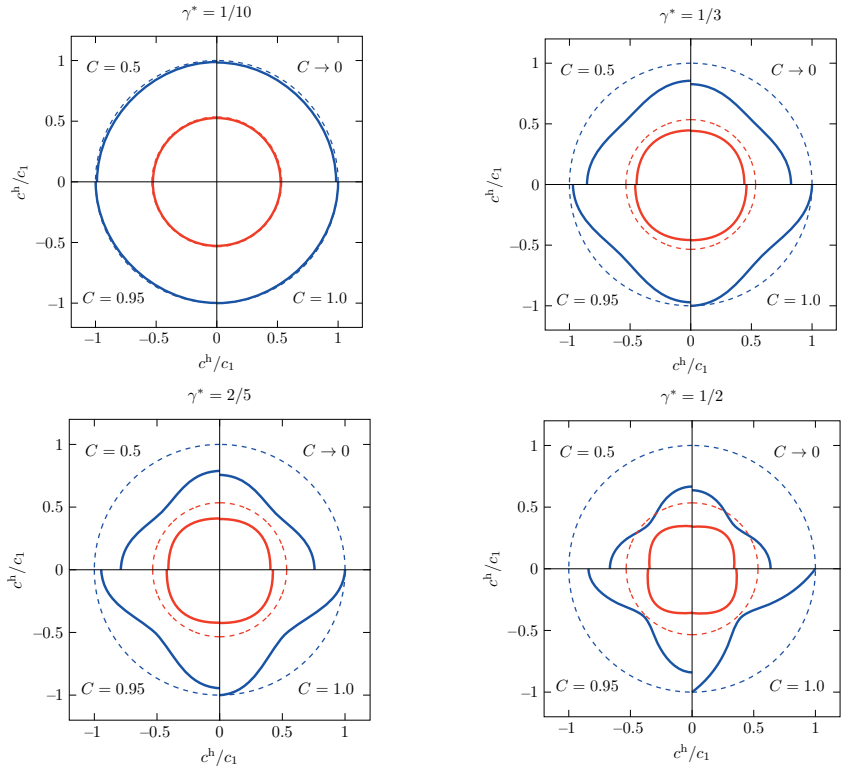

Fig. 18. Temporal spatial dispersion for a bilinear square 4-node element with a diagonal mass matrix for different mesh size to wave length ratios and for different Courant numbers for explicit time integration via the central difference method.

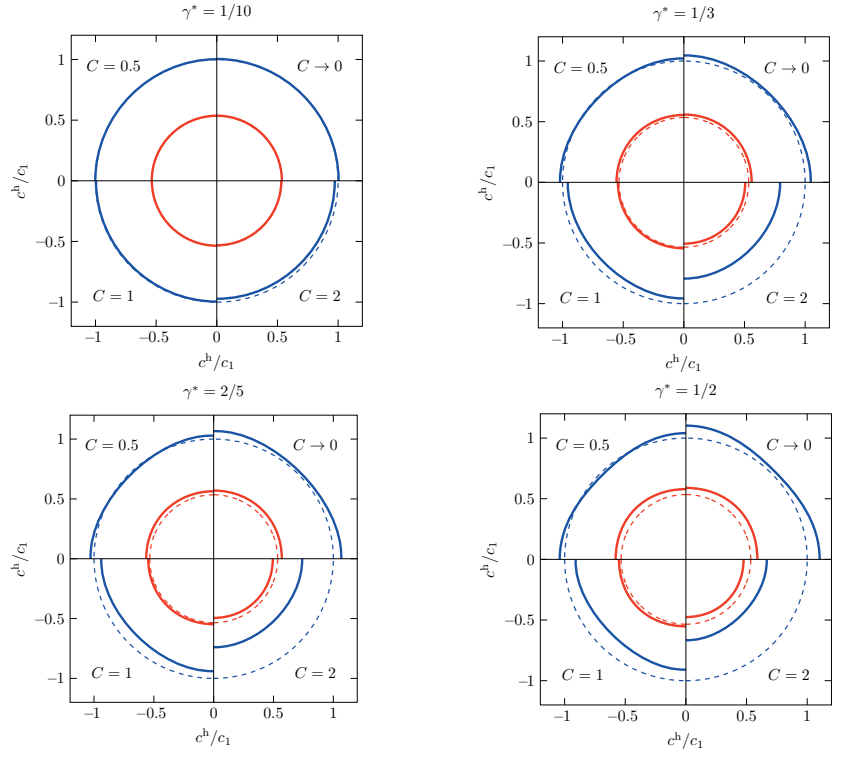

Fig. 19. Temporal spatial dispersion for a bilinear square 4-node element with a consistent mass matrix for different mesh size to wave length ratios and for different Courant numbers for implicit time integration via the averaged acceleration variant of the Newmark method.

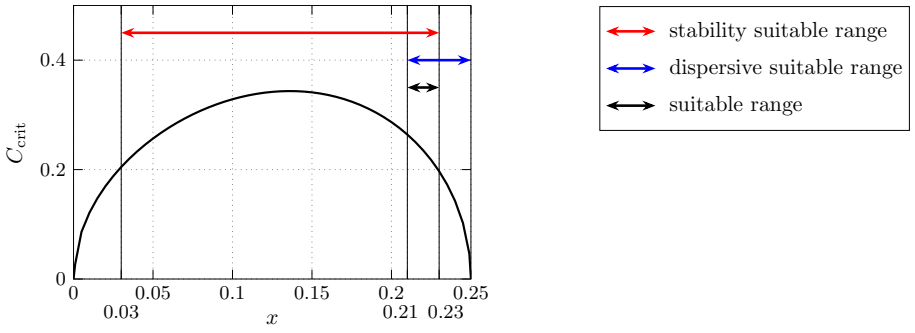

Fig. 20. Critical Courant number vs the mass distribution parameter.

5.5. Dispersion and mass matrix formulation

As is written in Section 3, diagonal (lumped) mass matrices are used in explicit time integration schemes. In Kolman et al. (2013), an 'optimum' lumped mass matrix for the studied finite element types is proposed, and the relationships suggesting the 'proper' choice of mesh size and timestep from the known frequency spectrum of the loading are presented. It is shown that in a plane regular mesh of square biquadratic finite elements, the corresponding element mass terms for midside nodes are recommended to be set up as $m_{\mathrm{mid}} = x \cdot m_{\mathrm{elem}}$, while the element mass terms for corner nodes are set up as $m_{\mathrm{corner}} = (0.25 - x) m_{\mathrm{elem}}$, where m_{elem} is the mass of the element and x is the so-called *mass distribution parameter*. The permissible interval of the mass parameter guaranteeing the preservation of the element mass is prescribed as $x \in (0, 0.25)$. To minimize the dispersion error for a square biquadratic finite element, the value $x = 0.23$ is derived and thus recommended (see Fig. 20).

5.6. Mesh size and timestep size suggestion

With respect to the temporal-spatial dispersion analysis of plane bilinear and biquadratic elements in *explicit* time integration by the central difference method, which is used for transient elastodynamics and wave propagation analysis, we suggest utilizing uniform finite element meshes and timesteps that satisfy the following conditions:

- for bilinear square finite elements: the element edge length $10H < \lambda_{\mathrm{min}}$, the mass matrix lumped by the 'row sum' method and the timestep given by $\Delta t = H/c_1$;
- for biquadratic square finite elements: the element edge length $5H < \lambda_{\mathrm{min}}$, the mass matrix lumped by the HRZ method and the timestep given by $\Delta t = 0.2H/c_1$.

Here, $\lambda_{\mathrm{min}} = c_1/f_{\mathrm{max}}$ marks an estimate of the minimum wave length of waves appearing in the problem to be solved, f_{max} is the maximum loading frequency given by the character of external loading and c_1 is the speed of a longitudinal wave. In principle, the value λ_{min} depends on the problem to be solved and on its loading characteristics and spectrum. It should be noted that determining the maximum loading frequency may be difficult since, in practice, the solved systems are not excited solely by periodic loadings. Also, the recommendation to employ regular (uniform) meshes in numerical computations of wave propagation problems in solids is very strong and not acceptable in many practical problems.

For *implicit* time integration by the average acceleration method, we suggest a suitable mesh size value given with respect to the wave length λ_{min} is:

- for bilinear square finite elements: the element edge length $10H < \lambda_{\mathrm{min}}$, the consistent mass matrix and the timestep given by $\Delta t = H/c_1$;
- for biquadratic square finite elements: the element edge length $5H < \lambda_{\mathrm{min}}$, the consistent mass matrix and the timestep given by $\Delta t = 0.5H/c_1$.

In making these recommendations, we set the numerical parameters of the FE model so that the temporal-spatial errors are smaller than 1%.

6. EXAMPLES OF WAVE PROPAGATION MODELLED BY 1D CONSTANT STRAIN FEM

This chapter shows the behaviour of a few classical numerical methods for the time integration of equations of motion describing stress wave propagation in a thin rod modelled by linear constant strain elements. The intention is to elucidate the dispersion side effects that result from spatial and temporal discretizations.

As a vehicle for the presentation, the simplest constant strain rod element is used. The local mass and stiffness matrices are described by Eqs (45), (46) and (47). The rod, assembled of uniform constant strain elements, is depicted in Fig. 21. Both sides of the rod are free, and the left side of the rod is loaded by the force with the given time history. No damping is considered. The equations of motion are described by a system of ordinary differential equations in the form $\mathbf{M}\ddot{\mathbf{q}} + \mathbf{K}\mathbf{q} = \mathbf{F}(t)$, where all the quantities are obtained by a suitable assembling process securing the conditions of displacement compatibility. For more details, see Okrouhlík and Höschl (1993).

The matrices $\mathbf{M}, \mathbf{K}$ are constant, the global accelerations $\ddot{\mathbf{q}}$, displacements $\mathbf{q}$ and external forces $\mathbf{F}$ are functions of time and space. The discretized equations of motion are subsequently solved by different methods for numerical integration in time. In this paragraph, the Newmark, the Houbolt (see Houbolt 1950), and the central difference methods are alternatively used. The time history of displacements, velocities and accelerations at chosen discrete time intervals $t, \Delta t, 2\Delta t, \ldots t_{\max}$, where Δt denotes the timestep, is observed.

The outlines and rules for the 'safe' usage of integration methods are generally advocated. Nevertheless, it might be of interest to analyse in detail the minute differences obtained by applying different integration methods to the same task.

In this text, the behaviour of integration procedures and finite elements when applied to studying waves in a thin rod are presented in pictorial form. 1D Lagrangian elements[4] with linear shape functions are used throughout. Consistent and diagonal mass matrix formulations are studied. All the kinematic and force quantities are computed and presented in their dimensionless forms (see Okrouhlík 2013), e.g. dimensionless time $\tau = 1$, when the wavefront reaches the end of the rod. When pulse length is discussed, it is understood that it is related to the time required for the wave to pass through the length of the rod. The computed quantities could be depicted either along the dimensionless length (from 0 to 1) of the rod or as functions of time (in timesteps) for a chosen node. The main identifiers accompanying the figures are:

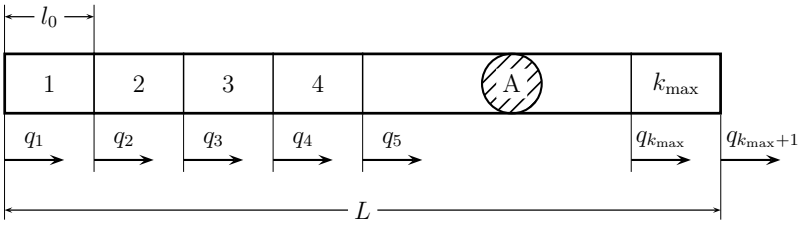

Fig. 21. Thin rod assembled of $k_{\max}$ uniform constant strain rod elements.

[4] Lagrangian, not Hermitian, polynomial approximation is used for displacement approximation.

t	time;
τ	dimensionless time with respect to the time the wave takes to pass through the bar;
Δt	timestep size of time integration;
type_of_loading	Heaviside pulse, rectangular pulse, half-sine pulse;
method_of_direct_time_int	Newmark, Houbolt, central differences;
type_of_mass_matrix	(cons) consistent, (diag) diagonal;
γ	Newmark artificial damping parameter;
x	position;
L	length of a bar;
hmts	number of timesteps the integration procedure requires to go through the length of the smallest element;
timp	length of pulse related to the time of wave propagation required to pass through the length of the bar.

The variable *hmts* used in this study is the reciprocal value of the Courant number, i.e. C = *wave speed* $\times$ *timestep/element size*.

Only a few cases are presented here. More details can be found in Okrouhlík (2013).

Study case 1 – Fig. 22

Parameters: 200 elements with a consistent mass matrix; half-sine pulse with time 'length' *timp* = 0.25 (related to the time required by the wave to pass the full length of the rod); central difference and Newmark methods with $\gamma = 0.5$ (indicating no algorithmic damping); timestep $\Delta t = 0.0025$, *hmts* = 2.

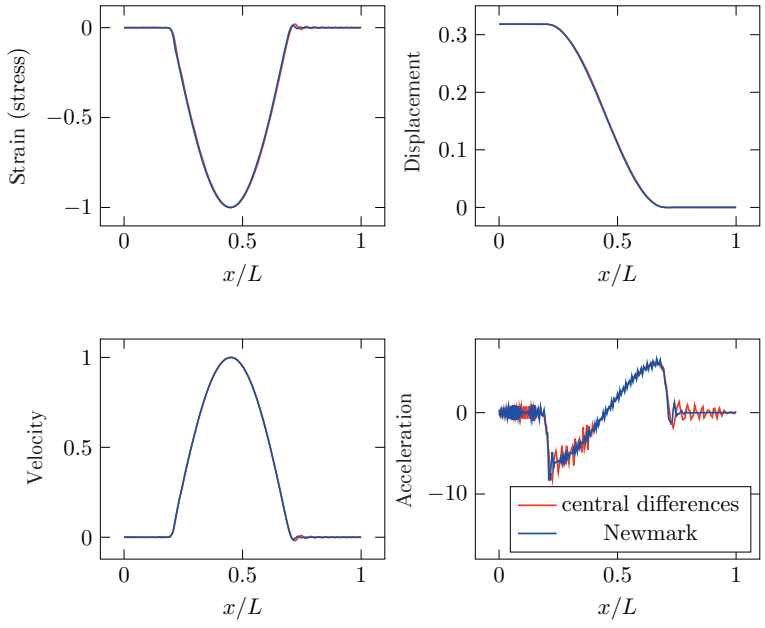

Fig. 22. Propagation of *sine pulse* through an elastic bar computed for 200 linear FE elements, the central difference method and the Newmark method with $\beta = 1/4$ and $\gamma = 0.5$ for the consistent mass matrix. Spurious signals are in the front of the wave. Other parameters: $\Delta t = 0.0025$, $htms = 2$, Courant number $C = 0.5$, dimensionless time $\tau = 0.7$.

In Fig. 22, one can see the FE response of the rod to the external half-sine pressure force pulse in time applied on the left-hand face of the rod. Such a force pulse induces a compression strain pulse in the rod, which propagates from left to right. The FE results should be mentally compared with those of an idealized 1D continuum represented by the wave equation (42), which, as a non-dispersive medium, would ensure that the introduced pulse (a half-sine pulse in this case) is propagated in an undistorted manner by the constant speed $c = \sqrt{E/\rho}$.

Figure 22 shows the distribution of strains, displacements, velocities and accelerations as they are distributed along the length of the rod. The picture is frozen at the moment when the wavefront reaches 0.7 of the length of the rod, which corresponds to the nondimensional time $\tau = 0.7$. The displacement distribution indicates that most of the body is at rest. The right-hand side of the rod (in front of the pulse) does not yet know that something has happened at its loaded face. But still, there is a visible nonzero signal in front of the wavefront, where, according to the wave equation, the rod should know nothing about the loading and be at absolute rest. The existence of these so-called spurious phenomena could be explained by conclusions stemming from the dispersion analysis for the consistent mass matrix formulation, which predicts a systematic *overestimation* of propagation speeds for higher frequencies.

The half-sine pulse, not being a harmonic function, has a continuous unbound spectrum – higher frequencies propagate faster and are thus overrunning the 'correct' wavefront.

Velocity distribution is easily understandable since it is the time derivative of displacement. Significant errors in acceleration are observed and are caused by the numerical magnification of velocity errors.

Study case 2 – Fig. 23

Note – similar case but with a diagonal mass matrix

When the rod is modelled by constant strain elements with a diagonal mass matrix formulation, the systematic *underestimation* of propagation speeds for higher frequencies can be observed. In this case, there is a visible nonzero signal behind the 'real' wavefront. See Fig. 23, where the strain results for the central difference method are presented.

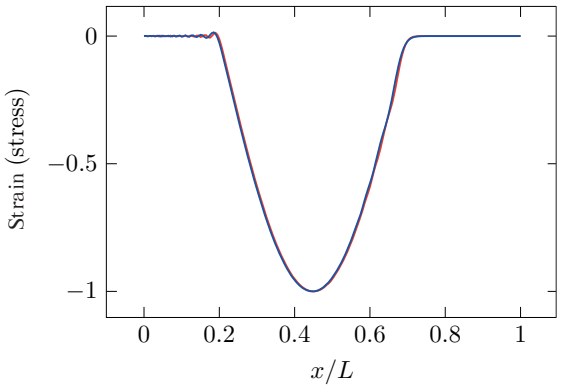

Fig. 23. Propagation of *sine pulse* through an elastic bar computed for 200 linear FE elements, the central difference method with a diagonal mass matrix – spurious signals are behind the wave. Other parameters: $\Delta t = 0.0025$, $htms = 2$, Courant number $C = 0.5$, dimensionless time $\tau = 0.7$.

Study case 3 – Fig. 24

There are 200 elements, a consistent mass matrix; rectangular pulse, *timp* = 0.25; central difference method and Newmark method with $\gamma = 0.5$; timestep size $\Delta t = 0.0025$, *hmts* = 2.

Let us observe (see Fig. 24) what happens when a rectangular pulse is being applied. The expected strain distribution (a rectangle) is 'spoiled' more than in the case of half-sine loading since the rectangular pulse contains more high frequency components than its half-sine counterpart. This is what the Fourier analysis predicts (see Stade 2005). The high-frequency components appearing in the solution are due to cumulative dispersion effects that always accompany the FE analysis. Instead of reasonable acceleration values, pure numerical litter is obtained. One is playing with fire when applying a loading pulse with discontinuities in time. We have done it intentionally. Application of any discontinuous loading function is actually the ultimate test of any time discretization method. Theoretically, displacements due to a rectangular pulse are functions of time possessing a sudden change of gradient. Velocity distribution (the time derivative of displacements) should have finite discontinuities in its distribution at locations corresponding to the sudden slope change in displacement distribution. Consequently, acceleration as the time derivative of velocity should contain the Dirac-type discontinuity at these locations. Such a condition is impossible to satisfy by any numerical computation.

In the 1D case, the Newmark method can be modified in such a way that the time and space discretization errors are cancelled out. It can be found in Subbaraj and Dokainish (1989) that due to a unique speed of wave propagation in a 1D elastic continuum, the corresponding FE model, discretized in time and space, has a *dispersionless* property for $\gamma = 0.5$, $\beta = 0.6$ and $htms = 1$ for the consistent mass matrix. This miraculous behaviour of strains is shown in Fig. 25 for a Heaviside pressure pulse, registered at dimensionless time $\tau = 0.7$. A dispersionless Newmark modification for 2D and 3D wave propagations was recently reported in the works of Cho et al. (2013), Kolman et al. (2016a) and Cho et al. (2019).

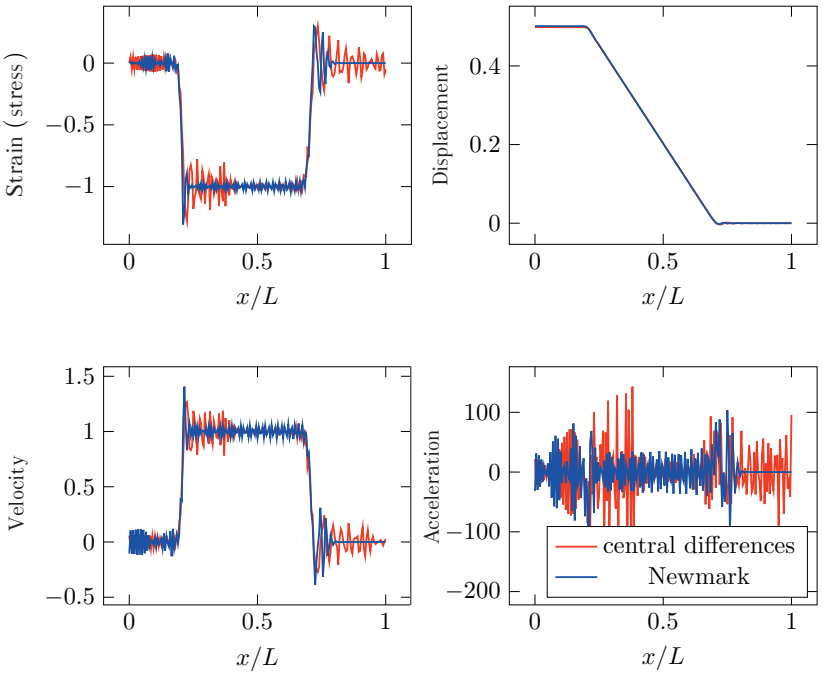

Fig. 24. Propagation of *rectangular pulse* through an elastic bar computed for 200 linear FE elements, the central difference method and the Newmark method with $\beta = 1/4$ and $\gamma = 0.5$ for the consistent mass matrix. Other parameters: $\Delta t = 0.0025$, $htms = 2$, Courant number $C = 0.5$, dimensionless time $\tau = 0.7$.

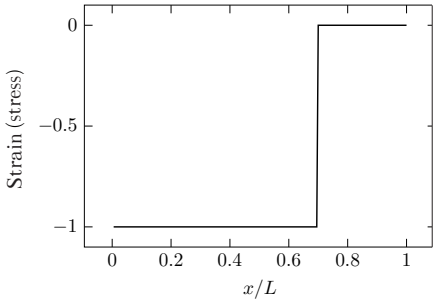

Fig. 25. Strain resultsfor *rectangular pulse* of the 'dispersionless' Newmark method with the parameters $\gamma = 0.5$, $\beta = 0.6$, a consistent mass matrix and *htms* = 1.

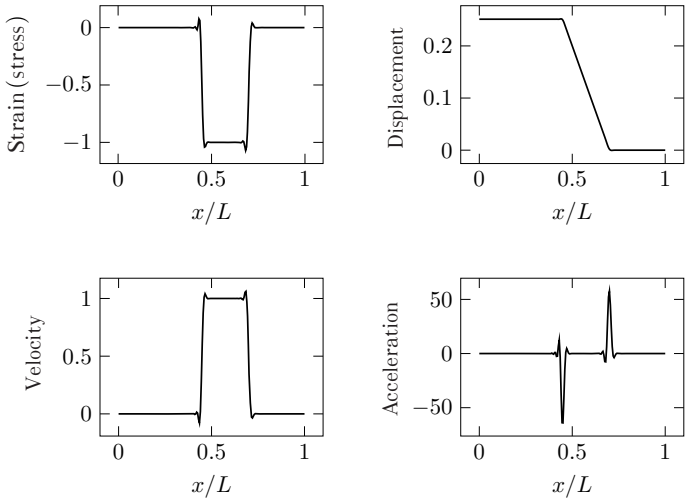

Fig. 26. Results of *sharp pulse* propagation in an elastic bar for the method mitigating spurious oscillations: diagonal mass matrix, $htms = 2$, Courant matrix $C = 0.5$.

One way to improve the temporal-spatial dispersion behaviour of finite element computation for discontinuous wave propagation is to employ the method for mitigating spurious oscillations presented by Park et al. (2012). In this method, the push-forward method and the central difference method are combined, and the spurious stress oscillations are suppressed with minimal numerical dissipation. This method has been extended into multidimensional wave propagation based on wave-component decomposition in Cho et al. (2013), Kolman et al. (2016a). The results of discontinuous wave propagation in a bar are shown in Fig. 26.

Study case 4 – Fig. 27

There are 200 elements, a consistent mass matrix; rectangular pulse with the time length $timp = 0.25$; Houbolt method and Newmark method with $\gamma = 0.6$; timestep size $\Delta t = 0.0025$, $htms = 2$.

A cosmetic effect, leading to partial eradication of high-frequency spurious frequencies, can be achieved by marching in time using the Newmark method with $\gamma > 0.5$, which introduces the so-called *algorithmic damping* into the solution. In this case, neither method of integration conserves energy. The results are presented in Fig. 27. Notice how 'nicely' the 'Dirac pulse singularity' is displayed in the acceleration distribution. It should be noted that both the Newmark method with numerical damping as well as the Houbolt method are not energetically conservative – they consume energy.

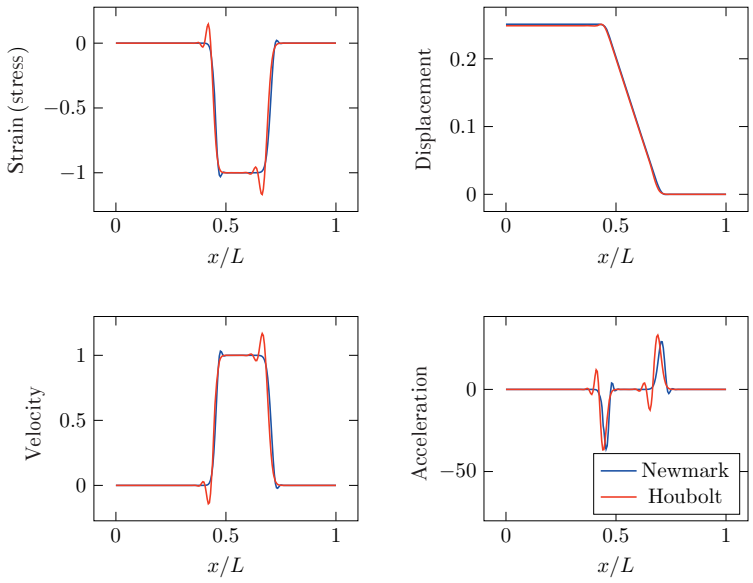

Fig. 27. Propagation of *rectangular pulse* through an elastic bar computed for 200 linear FE elements for the Houbolt method vs the Newmark method with algorithmic damping.

It was shown how the type of loading, the finite element formulation and the type of integration method influence the FE modelling process of stress wave propagation in a thin elastic rod. It is of the utmost importance to keep the high frequencies in the solution when impact tasks are analysed. To achieve this, diagonal mass matrices, explicit methods and smaller than critical timesteps are advocated.

Often, we deal with 'mild' loadings, where the high frequency components do not carry too much energy, and the corresponding modes, which are filtered out by using unconditionally stable methods with large timesteps, do not considerably spoil the solution. Energy checks might always be useful.

The rectangular pulse, used in the above testing, contains discontinuities. As such, it does not appear in nature, and to model it numerically is a sort of computational crime. But it represents the ultimate standard for rough testing integration procedures. When modelling transient phenomena by finite elements, discretization errors cannot be fully eliminated, only suppressed to a certain extent.

The literature devoted to this subject is voluminous. For further study, see Goudreau and Taylor (1973), Hulbert and Hughes (1990), Hughes and Liu (1978), Chung and Hulbert (1993), Lew et al. (2004), Park et al. (2012), Bathe and Noh (2012), Hughes (2000), Belytschko et al. (2000).

7. CONCLUSIONS

Dispersion is a phenomenon characterized by the fact that the speed of wave propagation depends on its frequency. The unbound solid elastic continuum is thus declared as the perfect dispersionless medium since all the harmonic stress waves propagate at the same speed, regardless of their frequencies. The propagation of stress waves in elastic solid continua is described by partial differential equations of motion expressed in spatial and temporal coordinates. The finite element method replaces the infinitesimally fine structure of a continuum with small parts – elements of finite size. This process is called the discretization in space (sometimes semidiscretization) and produces ordinary differential equations instead. The dispersion analysis is based on observing the differences between the vibration responses within continuous and semidiscretized objects. The analysis (i.e. the assessment of differences called the dispersion errors) is provided both analytically and numerically. The latter approach leads to the generalized eigenvalue problem. This part of the analysis, where finite element size plays an important role and the time variable is merely a parameter, leads to the *spatial dispersion* explanation.

When the time response of a semidiscretized body to a transient excitation is analysed, it is necessary to solve the resulting equations of motion (having the form of ordinary differential equations) numerically, applying various step by step integration procedures. This way, the time response of a body is obtained not continuously, but at discrete time intervals, separated by so-called timesteps. This part of the analysis, where errors arising from time discretization are assessed, explains the phenomenon of *temporal dispersion*.

In this paper, the classical approach to the assessment of spatial and temporal dispersion is complemented by the so-called spatial-temporal dispersion analysis, suggesting practical steps toward reliable finite element modelling of transient tasks in solid continuum mechanics. To limit the discretization errors, one must not only minimize the timestep and the mesh size but also correctly relate the choice of time integration operators with mass matrix formulations (as well as take into account the frequency spectrum of the loading).

The dispersion analysis is devoted to 1D and 2D finite elements, both for linear and quadratic displacement approximations. The following items are presented in detail:

- Compared to the infinitely long frequency spectrum in an ideal continuum, the finite element frequency spectrum is bounded and limited by the so-called cut-off frequencies. This means that the high-frequency components of the propagating signal are filtered out. The frequency limits for consistent mass matrices are higher than those for diagonal mass matrices.
- With respect to the speed of wave propagation of an ideal continuum, the speed of wave propagation in a finite element model is **overestimated** when the **consistent mass matrix** formulation is used. It is **underestimated** with the **diagonal mass matrix** formulation.
- In 2D and 3D spaces, discretization-induced anisotropy is observed.
- Time integration methods behave as high-frequency filters as well. The high-frequency components of propagating waves are filtered out.
- Explicit integration methods are conditionally stable only. The integration process has to proceed in time by integration steps Δt that are smaller than the so-called critical timestep Δt_{crit}. Not satisfying this condition leads to an unbound numerical response.
- Different ways to estimate the critical timestep are presented. Generally, the *computing speed* should not be higher than the *wave speed*.
- The dimensionless timestep, defined as C = *wave speed* $\times$ *timestep/element size* and called the Courant number, plays an important role when assessing discretization errors in space and time.
- Implicit integration methods are unconditionally stable. Although any timestep could be used, a physically accurate modelling of time response would not be guaranteed.
- The temporal discretization errors of the central difference method (representing the explicit methods) and the spatial discretization errors of the diagonal mass matrix formulation produce errors of opposite signs, which have a tendency to cancel each other out. The same favourable situation exists for the Newmark method (representing the implicit methods) when used in combination with a consistent mass matrix formulation.

For higher-order elements, where displacements are approximated by higher-order Lagrangian polynomials, the following conclusions are observed:

- Dispersion analysis of higher-order elements for *optical modes* tends to reveal unrealistic wave behaviour. One can increase the cut-off limit for the highest available frequency, but this comes at the expense of increased computing costs.
- Dispersion diagrams consist of distinct branches that are separated by certain frequency regions (sometimes called *bandpass filters*) through which the harmonic waves of particular frequencies cannot propagate. These waves are strongly attenuated. Mathematically, the description of waves in these regions changes from that of a vibrating to an exponential character. Attenuation has nothing in common with damping; it is not accompanied by a loss of energy.
- To minimize dispersion errors due to the diagonalization of mass matrices for a square biquadratic finite element, the value of the so-called *mass distribution parameter* is derived. It is shown how the type of mass matrix diagonalization influences the displacement behaviour.

- Dispersion results are compared for 4-node bilinear elements and for 8-node biquadratic elements with diagonal mass matrices of different mesh size to wave length ratios and different Courant numbers.
- With respect to the temporal-spatial dispersion analysis of plane bilinear and biquadratic elements in explicit time integration, used for transient elastodynamics and wave propagation analysis, uniform finite element meshes are suggested and timesteps are recommended.

In practical engineering computations, we do not deal with the propagation of monochromatic harmonic waves but with finite-length pulses of various shapes. And these, viewing them through the prism of the Fourier analysis, are composed of infinitely many harmonics whose frequencies range from zero to infinity. Also, establishing the 'optimum' value of the element size and the timestep depends on the frequency spectrum of the loading.

ACKNOWLEDGEMENTS

The work has been supported by the grant project GA23-04676J of the Czech Science Foundation (CSF) within institutional support RVO:61388998 and realized under the Czech–Estonian mobility project EstAV-21-02. The publication costs of this article were partially covered by the Estonian Academy of Sciences.

Photo: private collection

Assoc. Prof. Radek Kolman
Education
2009 PhD, Faculty of Mechanical Engineering, Czech Technical University (CTU) in Prague; Mechanics of Solids, Deformable Bodies and Continua
2002 Ing. (MEng), Faculty of Mechanical Engineering, CTU in Prague; Applied Mechanics
Academic and professional positions
Since 2022 Associate Professor, Faculty of Transportation Sciences, CTU in Prague
2021–2022 Lecturer, Faculty of Transportation Sciences, CTU in Prague
2018–2022 Head of Department of Technical Studies, Docent, The College of Polytechnics Jihlava
2013–2021 Head of the Laboratory of Computational Solid Mechanics, Institute of Thermomechanics, Czech Academy of Sciences (CAS)
2009–2013 Scientist, Institute of Thermomechanics, CAS
2004–2009 Structural Engineer and Designer, Agrostroj Pelhřimov LLC
2003–2009 PhD student, Institute of Thermomechanics, CAS
Consulting and teaching roles
2020–2023 Consultant of Numerical Methods, FEMconsulting LLC
2018–2022 Lecturer, The College of Polytechnics Jihlava

Photo: private collection

Dr. Alena Kruisová
Education
2003 PhD, Faculty of Mechanical Engineering, Czech Technical University (CTU) in Prague; PhD thesis: Constitutive Modelling of Hyperelastic Materials Using the Logarithmic Description
1995 Master's degree, Faculty of Mechanical Engineering, CTU in Prague; Applied Mechanics
Academic and professional positions
Since 1995 Scientist, Institute of Thermomechanics, Czech Academy of Sciences (CAS)
1998–1999 Research Fellow, Computational Mechanics Group, Faculty of Civil Engineering and Geosciences, TU Delft, Netherlands
1995–1998 Stress Analyst (part-time), Vamet Ltd
Research interests
Computational mechanics
Stress wave propagation
Finite elements
Hyperelastic materials modelling
Material models in acoustoelasticity

Photo: private collection

Prof. Miloslav Okrouhlík
Education
2008 Professor, Faculty of Nuclear Sciences and Physical Engineering, Czech Technical University (CTU) in Prague
1969 MScA, École Polytechnique, Montreal, Canada
1963 Graduated from the Faculty of Mechanical Engineering, CTU in Prague
Academic and professional positions
Since 1970 presently: Professor Emeritus; formerly: researcher and head of department, Institute of Thermomechanics, Czech Academy of Sciences (CAS)
Since 1979 Lecturer, University of Ústí nad Labem, Technical University of Liberec, Jihlava Polytechnic Institute
2001–2013 Researcher and lecturer, University of Uppsala, Sweden
1963–1968 Lecturer, Department of Technical Mechanics, Faculty of Mechanical Engineering, CTU in Prague
Leadership roles
2008–2017 Chairman, Czech Society of Mechanics
1998–2005 Secretary General, EUROMECH Society
1994–2002 Head of Department of Solid Mechanics, Institute of Thermomechanics, CAS
Research interests
Stress wave propagation
Finite elements
Continuum and computational mechanics
Recent highlight
2024 Author of the Year for book Mechanics of Deformable Bodies*, downloaded 12 055 times from website of the Technical University of Liberec*

REFERENCES

Abboud, N. and Pinsky, P. M. 1992. Finite element dispersion analysis for the three-dimensional second-order scalar wave equation. *Int. J. Numer. Methods Eng.*, **35**(6), 1183–1218.

Achenbach, J. D. 1973. *Wave Propagation in Elastic Solids*. North-Holland Pub. Co., Amsterdam.

Bathe, K.-J. 1996. *Finite Element Procedures*. Prentice-Hall, Englewood Cliffs, New Jersey.

Bathe, K.-J. and Noh, G. 2012. Insight into an implicit time integration scheme for structural dynamics. *Comput. Struct.*, **98–99**, 1–6.

Bažant, Z. P. and Celep, Z. 1982. Spurious reflection of elastic waves in nonuniform meshes of constant and linear strain unite elements. *Comput. Struct.*, **15**(4), 451–459.

Belytschko, T. and Hughes, T. J. R. (eds). 1983. Computational Methods for Transient Analysis. In *Computational Methods in Mechanics*. **1**. North-Holland Pub. Co., Amsterdam, New York.

Belytschko, T. and Mullen, R. 1978. On dispersive properties of finite element solutions. In *Modern Problems in Elastic Wave Propagation* (Miklowitz, J. and Achenbach, J., eds). John Wiley and Sons, 67–82.

Belytschko, T., Liu, W. K. and Moran, B. 2000. *Nonlinear Finite Elements for Continua and Structures*. John Wiley and Sons, Chichester.

Benson, D. J. 1998. Stable time step estimation for multi-material Eulerian hydrocodes. *Comput. Methods Appl. Mech. Eng.*, **167**(1–2), 91–205.

Brepta, R. and Okrouhlík, M. 1984. *Dispersion properties of a plane continuum model consisted of rectangular triangular finite elements*. Research report Z-966/84. Institute of Thermomechanics, Prague, Czech Republic.

Brepta, R. and Okrouhlík, M. 1986. *Dispersive properties of rectangular and square element in 2D regions*. Research report Z-998/86. Institute of Thermomechanics, Prague, Czech Republic.

Brepta, R., Okrouhlík, M. and Valeš, F. 1985. *Wave Propagation and Impact Phenomena in Solids and Methods of Solution*. Academia, Prague, Czech Republic.

Brepta, R., Valeš, F., Červ, J. and Tikal, B. 1996. Rayleigh wave dispersion due to spatial (FEM) discretization of a thin elastic solid having non-curved boundary. *Comput. Struct.*, **58**(6), 1233–1244.

Brillouin, L. 1953. *Wave Propagation in Periodic Structures*. Dover Publication, New York.

Celep, Z. and Bažant, Z. P. 1983. Spurious reflection of elastic waves due to gradually changing finite element size. *Int. J. Numer. Methods Eng.*, **19**(5), 631–646.

Červ, J., Brepta, R., and Valeš, F. 1996. Acoustic surface waves in media discretized by FEM. *Acustica*, **82**(1), 235.

Červ, J., Adámek, V., Valeš, F., Gabriel, D. and Plešek, J. 2016. Wave motion in a thick cylindrical rod undergoing longitudinal impact. *Wave Motion*, **66**, 88–105.

Chin, R. C. Y. 1975. Dispersion and Gibbs phenomenon associated with difference approximations to initial boundary-value problems for hyperbolic equations. *J. Comput. Phys*, **18**(3), 233–247.

Cho, S. S., Park, K. C. and Huh, H. 2013. A method for multidimensional wave propagation analysis via component-wise partition of longitudinal and shear waves. *Int. J. Numer. Methods Eng.*, **95**(3), 212–237.

Cho, S. S., Kolman, R., González, J. A. and Park, K. C. 2019. Explicit multistep time integration for discontinuous elastic stress wave propagation in heterogeneous solids. *Int. J. Numer. Methods Eng.*, **118**(5), 276– 302.

Chopra, A. K. 2001. *Dynamics of Structures*. Prentice-Hall, New York, USA.

Christon, M. A. 1999. The influence of the mass matrix on the dispersive nature of the semi-discrete, second-order wave equation. *Comput. Methods Appl. Mech. Eng.*, **173**(1), 147–166.

Chung, J. and Hulbert, G. M. 1993. A time integration algorithm for structural dynamics with improved numerical dissipation: the generalized-α method. *J. Appl. Mech.*, **60**(2), 371–375.

Cottrell, J. A., Reali, A., Bazilevs, Y. and Hughes, T. J. R. 2006. Isogeometric analysis of structural vibrations. *Comput. Methods Appl. Mech. Eng.*, **195**(41–43), 5257–5296.

Courant, R. 1943. Variational methods for the solution of problems of equilibrium and vibrations. *Bull. Amer. Math. Soc.*, **49**, 1–23.

Dauksher, W. and Emery, A. F. 1997. Accuracy in modeling the acoustic wave equation with Chebyshev spectral finite elements. *Finite Elem. Anal. Des.*, **26**(2), 115–128.

Dauksher, W. and Emery, A. F. 2000. The solution of elastostatic and elastodynamic problems with Chebyshev spectral finite elements. *Comput. Methods Appl. Mech. Eng.*, **188**(1), 217–233.

Davies, R. M. 1956. Stress waves in solids. *Br. J. Appl. Phys.*, **7**(6), 203–209.

Dokainish, M. A. and Subbaraj, K. 1989. A survey of direct time-integration methods in computational structural dynamics – I. Explicit methods. *Comput. Struct.*, **32**(6), 1371–1386.

Engelbrecht, J. 2015. *Questions About Elastic Waves*. Springer, Cham.

Felippa, C. A., Guo, Q. and Park, K. C. 2015. Mass matrix templates: general description and 1D examples. *Arch. Comput. Methods Eng.*, **22**, 1–65.

Fried, I. 1972. Bounds on the extremal eigenvalues of the finite element stiffness and mass matrices and their spectral condition number. *J. Sound Vib.*, **22**(4), 407–418.

Gershgorin, S. 1931. Uber die Abgrenzung der Eigenwerte einer Matrix (On the delimitation of the eigenvalues of a matrix). *Izv. Akad. Nauk SSSR, Serija Matematika*, **7**(3), 749–754.

Goudreau, G. L. and Taylor, R. L. 1973. Evaluation of numerical integration methods in elastodynamics. *Comput. Methods Appl. Mech. Eng.*, **2**(1), 69–97.

Hallquist, O. J. 2006. *LS-DYNA Theoretical Manual*. LST, Livermore.

Hilber, H. M., Hughes, T. J. R. and Taylor, R. L. 1977. Improved numerical dissipation for time integration algorithms in structural dynamics. *Earthq. Eng. Struct. Dyn.*, **5**(3), 283–292.

Hinton, E., Rock, T. and Zienkiewicz, O. C. 1976. A note on mass lumping and related processes in the finite element method. *Earthq. Eng. Struct. Dyn.*, **4**(3), 245–249.

Holmes, N. and Belytschko, T. 1976. Postprocessing of finite element transient response calculations by digital filters. *Comput. Struct.*, **6**(3), 211–216.

Houbolt, J. C. 1950. A recurrence matrix solution for the dynamic response of elastic aircraft. *J. Aeronaut. Sci.*, **17**(9), 540–550.

Hrennikoff, A. 1941. Solution of problems of elasticity by the framework method. *J. Appl. Mech*., **8**(4), A169–A175.

Hughes, T. J. R. 2000. *The Finite Element Method: Linear Static and Dynamic Finite Element Analysis*. Dover Publication, Mineola, NY.

Hughes, T. J. R. and Liu, W. K. 1978. Implicit-explicit finite elements in transient analysis: stability theory. *J. Appl. Mech.*, **45**(2), 371–374.

Hughes, T. J. R., Reali, A. and Sangalli, G. 2008. Duality and unified analysis of discrete approximations in structural dynamics and wave propagation: comparison of *p*-method finite elements with *k*-method NURBS. *Comput. Methods Appl. Mech. Eng.*, **197**(49–50), 4104–4124.

Hulbert, G. M. and Hughes, T. J. R. 1990. Space-time finite element methods for second-order hyperbolic equations. *Comput. Methods Appl. Mech. Eng.*, **84**(3), 327–348.

Kolman, R., Plešek, J., Okrouhlík, M. and Gabriel, D. 2013. Grid dispersion analysis of plane square biquadratic serendipity finite elements in transient elastodynamics. *Int. J. Numer. Methods Eng.*, **96**(1), 1–28.

Kolman, R., Plešek, J. and Okrouhlík, M. 2014. Complex wavenumber Fourier analysis of the B-spline based finite element method. *Wave Motion*, **51**(2), 348–359.

Kolman, R., Cho, S. S. and Park, K. C. 2016a. Efficient implementation of an explicit partitioned shear and longitudinal wave propagation algorithm. *Int. J. Numer. Methods Eng.*, **107**(7), 543–579.

Kolman, R., Plešek, J., Červ, J., Okrouhlík, M. and Pařík, P. 2016b.Temporal-spatial dispersion and stability analysis of finite element method in explicit elastodynamics. *Int. J. Numer. Methods Eng.*, **106**(2), 113–128.

Kolman, R., Okrouhlík, M., Berezovski, A., Gabriel, D., Kopačka, J. and Plešek, J. 2017. B-spline based finite element method in one-dimensional discontinuous elastic wave propagation. *Appl. Math. Model.*, **46**, 382–395.

Kolsky, H. 1953. *Stress Waves in Solids*. Clarendon Press, Oxford.

Krieg, R. D. and Key, S. W. 1973. Transient shell response by numerical time integration. *Int. J. Numer. Methods Eng.*, **7**(3), 273–286.
Kruisová, A., Kolman, R., Mračko, M. and Okrouhlík, M. 2019. Temporal-spatial dispersion analysis of finite element method in implicit time integration. In *Engineering Mechanics 2019* (Zolotarev, I. and Radolf, V., eds), **25**, 215–218.
Kulak, R. F. 1989. *Critical time step estimation for three-dimensional explicit impact analysis*. Progress report. Argonne National Laboratory, Argonne, Illinois.
Kwok, W. Y., Moser, R. D. and Jiménez, J. 2001. A critical evaluation of the resolution properties of B-spline and compact finite difference methods. *J. Comput. Phys.*, **174**(2), 510–551.
Lew, A., Marsden, J. E., Ortiz, M. and West, M. 2004. Variational time integrators. *Int. J. Numer. Methods Eng.*, **60**(1), 153–212.
Liu, J. B., Sharan, S. K. and Yao, L. 1994. Wave motion and its dispersive properties in a finite element model with distortional elements. *Comput. Struct.*, **52**(2), 205–214.
Love, A. E. H. 1944. *A Treatise on the Mathematical Theory of Elasticity*. Dover Publications, New York.
Marfurt, K. J. 1984. Accuracy of finite-difference and finite-element modeling of the scalar and elastic wave equations. *GEOPHYSICS*, **49**(5), 533–549.
Mullen, R. and Belytschko, T. 1982. Dispersion analysis of finite element semidiscretizations of the two-dimensional wave equation. *Int. J. Numer. Methods Eng.*, **18**(1), 11–29.
Newmark, N. M. 1959. Method of computation for structural dynamics. *J. Eng. Mech. Div.*, **85**(3), 67–94.
Okrouhlík, M. 1994. Special issue on mechanics of contact impact. *Appl. Mech. Rev.*, **47**(2), 34.
Okrouhlík, M. 2013. Dispersion and time integration schemes in finite-element analysis – a practical pictorial manual. *Int. J. Mech. Eng. Educ.*, **41**(1), 44–71.
Okrouhlík, M. and Höschl, C. 1993. A contribution to the study of dispersive properties of one-dimensional Lagrangian and Hermitian elements. *Comput. Struct.*, **49**(5), 779–795.
Okrouhlík, M. and Pták, S. 2005. Assessment of experiment by finite element analysis: comparison, self-check and remedy. *Strojnický časopis*, **56**(1), 18–39.
Park, K. C. 1977. Practical aspects of numerical time integration. *Comput. Struct.*, **7**(3), 343–353.
Park, K. C., Lim, S. J. and Huh, H. 2012. A method for computation of discontinuous wave propagation in heterogeneous solids: basic algorithm description and application to one-dimensional problems. *Int. J. Numer. Methods Eng.*, **91**(6), 622–643.
Schreyer, H. 1983. Dispersion of semidiscretized and fully discretized systems. In *Computational Methods for Transient Analysis* (Belytschko, T. and Hughes, T., eds). North-Holland Pub. Co., Amsterdam, New York, 267–299.
Seriani, G. 2004. Double-grid Chebyshev spectral elements for acoustic wave modeling. *Wave Motion*, **39**(4), 351–360.
Seriani, G. and Oliveira, S. P. 2008. Dispersion analysis of spectral element methods for elastic wave propagation. *Wave Motion*, **45**(6), 729–744.
Stade, E. 2005. *Fourier Analysis*. John Wiley and Sons, Hoboken, Chichester.
Stein, E., de Borst, R. and Hughes, T. J. R. 2017. *Encyclopedia of Computational Mechanics*. John Wiley and Sons, Chichester.
Subbaraj, K. and Dokainish, M. A. 1989. A survey of direct time-integration methods in computational structural dynamics – II. Implicit methods. *Comput. Struct.*, **32**(6), 1387–1401.
Thompson, L. L. and Pinsky, P. M. 1995. Complex wave-number Fourier-analysis of the *p*-version finite element method. *Comput. Mech.*, **13**, 255–275.
Vichnevetsky, R. and Bowles, J. 1982. *Fourier Analysis of Numerical Approximations of Hyperbolic Equations*. Society for Industrial and Applied Mathematics, Philadelphia, PA.
Zienkiewicz, O. C. 1971. *The Finite Element Method in Engineering Science*. McGraw-Hill, London, New York.
Zukas, J. A. 1990. *High Velocity Impact Dynamics*. Wiley, New York.

Ülevaade lineaarsete elastsete lainete modelleerimisest ning esimest ja teist järku lõplike elementide ajalis-ruumiline dispersioon

Radek Kolman, Miloslav Okrouhlík ja Alena Kruisová

Artiklis on vaatluse all elastse lainelevi modelleerimine tahkistes lõplike elementide meetodil. Pideva ruumi ja aja diskreetimine toob paratamatult kaasa numbrilise dispersiooni tekke ning seetõttu ei anna lõplike elementide meetod lainelevi ülesannete puhul täiesti täpseid tulemusi. Toetudes oma uuringutele, näitavad autorid, et numbrilisest dispersioonist tekkivaid ebatäpsusi saab minimeerida, kasutades optimaalses koguses elemente. Artiklis antakse konkreetseid soovitusi diskreetse arvutusskeemi valikuks.